Pergamon

Geochimica et Cosmochimica Acta, Vol. 68, No. 15, pp. 3171–3187, 2004

0016-7037/04 $30.00 + .00

doi:10.1016/j.gca.2003.10.024

Reduction of TcO_4^- by sediment-associated biogenic Fe(II)

JAMES K. FREDRICKSON,[1,*] JOHN M. ZACHARA,[1] DAVID W. KENNEDY,[1] RAVI K. KUKKADAPU,[1] JAMES P. MCKINLEY,[1] STEVE M. HEALD,[1,2] CHONGXUAN LIU,[1] and ANDREW E. PLYMALE[1]

[1]Pacific Northwest National Laboratory, P.O. Box 999, MSIN P7-50, Richland, WA 99352, USA
[2]Argonne National Laboratory, Argonne, IL 60439, USA

(*Received June* 13, 2003; *accepted in revised form October* 14, 2003)

Abstract—The potential for reduction of $^{99}TcO_{4\,(aq)}^-$ to poorly soluble $^{99}TcO_2 \cdot nH_2O_{(s)}$ by biogenic sediment-associated Fe(II) was investigated with three Fe(III)-oxide containing subsurface materials and the dissimilatory metal-reducing subsurface bacterium *Shewanella putrefaciens* CN32. Two of the subsurface materials from the U.S. Department of Energy's Hanford and Oak Ridge sites contained significant amounts of Mn(III,IV) oxides and net bioreduction of Fe(III) to Fe(II) was not observed until essentially all of the hydroxylamine HCl-extractable Mn was reduced. In anoxic, unreduced sediment or where Mn oxide bioreduction was incomplete, exogenous biogenic $TcO_2 \cdot nH_2O_{(s)}$ was slowly oxidized over a period of weeks. Subsurface materials that were bioreduced to varying degrees and then pasteurized to eliminate biological activity, reduced $TcO_{4\,(aq)}^-$ at rates that generally increased with increasing concentrations of 0.5 N HCl-extractable Fe(II). Two of the sediments showed a common relationship between extractable Fe(II) concentration (in mM) and the first-order reduction rate (in h^{-1}), whereas the third demonstrated a markedly different trend. A combination of chemical extractions and ^{57}Fe Mössbauer spectroscopy were used to characterize the Fe(III) and Fe(II) phases. There was little evidence of the formation of secondary Fe(II) biominerals as a result of bioreduction, suggesting that the reactive forms of Fe(II) were predominantly surface complexes of different forms. The reduction rates of $Tc(VII)O_4^-$ were slowest in the sediment that contained plentiful layer silicates (illite, vermiculite, and smectite), suggesting that Fe(II) sorption complexes on these phases were least reactive toward pertechnetate. These results suggest that the in situ microbial reduction of sediment-associated Fe(III), either naturally or via redox manipulation, may be effective at immobilizing $TcO_{4\,(aq)}^-$ associated with groundwater contaminant plumes.

1. INTRODUCTION

^{99}Tc is a long-lived ($t^{1/2} = 2.13 \times 10^5$ y) fission product unique to nuclear production, reprocessing, or natural fission. It exists as an important subsurface contaminant at numerous U.S. Department of Energy sites including Hanford, Washington; Oak Ridge, Tennessee; Paducah, Kentucky; and others (Riley and Zachara, 1992). ^{99}Tc migrates rapidly with vadose zone water and groundwater as the mobile pertechnetate [$Tc(VII)O_4^-$] anion (see, for example, Serne et al., 2001a; Serne et al., 2001b; Serne et al., 2001c). It is weakly sorbed under most geochemical conditions. At the Hanford Site, four large ^{99}Tc groundwater plumes exist and new ones are forming as ^{99}Tc released to cribs and leaked from single-shell high-level waste tanks migrates through the vadose zone. Over 40 Ci of $Tc(VII)O_4^-$ are forecast to discharge to the Columbia River in future years, making it one of the site's major risk-driving contaminants.

The electrode potential of the Tc(VII)-Tc(IV) couple, $TcO_4^- + 4H^+ + 3e^- = TcO_2 - (nH_2O_{(s)} + (2-n)H_2O_{(l)}$, ranges between 0.738 and 0.786 V depending on the crystallinity and hydration (n) of the oxide, and the conditions of measurement. The most reliable average value for the E^o of the couple has been reported as 0.746 V [log K(298 K) = 37.8] (Rard et al., 1999). Under anoxic conditions some microorganisms including *Geobacter metallireducens* (Lloyd and Macaskie, 1996), *Shewanella putrefaciens* (Wildung et al., 2000), *Desulfovibrio desulfuricans* (Lloyd et al., 1999), and *Escherichia coli* (Lloyd et al., 1997) can couple the oxidation of H_2 or organic compounds to the reduction of $Tc(VII)O_{4\,(aq)}^-$ to an insoluble oxide [$Tc(IV)O_2 \cdot nH_2O$]. Although microbial reduction has been demonstrated to be an effective process for the ex situ treatment of Tc contaminated wastewaters (Lloyd et al., 1999), the effectiveness of this process for the in situ reduction and immobilization of Tc in the subsurface is less certain.

Fe(III) and Mn(III/IV) oxides are common reactive components of aerobic soils and sediments, and Fe(III) oxides in particular can constitute a substantial redox buffering capacity in aquifer sediments (Heron and Christensen, 1995). Hence, the in situ reduction and subsequent immobilization of redox sensitive contaminants such as Tc can be complicated by the presence of reactive metal oxides. Fe(III) and Mn(III/IV) oxides can retard the microbial reduction of contaminants via competition as a terminal electron acceptor (Wielinga et al., 2000) or by oxidizing biologically reduced metals or radionuclides (Fredrickson et al., 2002; Liu et al., 2002). Alternatively, the presence of crystalline Fe(III) oxides may have relatively little impact on the rate and extent of contaminant reduction by metal-reducing bacteria (Fredrickson et al., 2000; Wielinga et al., 2000) and may even facilitate reduction by forming reactive surface complexes with Fe(II) (Liger et al., 1999). Nanocrystalline magnetite, as a product of microbially reduced ferrihydrite, has also been shown to reduce Tc(VII) to an insoluble form, and it has been suggested that the indirect reduction of $Tc(VII)O_{4\,(aq)}^-$ via biogenic Fe(II) may be an environmentally important pathway (Lloyd et al., 2000). Whether metal oxides retard, promote, or have no impact on the reduction of contam-

* Author to whom correspondence should be addressed (jim.fredrickson@pnl.gov).

inants is largely dependent upon their mineralogy and free energy, surface area and surface properties, and physical distribution within sediments.

The purpose of this research was to investigate the biologic reduction of Fe(III) and Mn(III/IV) oxides in natural sediments from contrasting geochemical environments and to determine the reactivity of these bioreduced sediments with regard to Tc(VII) reduction. The nature of the reactive Fe(II) is explored as is the form and distribution of the reduced Tc. This information contributes to the understanding of the role of biogenic Fe(II) in the reductive immobilization of Tc(VII) and provides insights into potential strategies for the in situ immobilization of redox sensitive metal and radionuclide contaminants.

2. MATERIAL AND METHODS

2.1. Soils and Sediments

Semiconsolidated Pliocene-age fluvial sediment from the upper Ringold Formation near the Hanford Site was sampled from the White Bluffs approximately 60 m above the Columbia River. This material is referred to as Ringold 6-6/6-7. Almost all $^{99}Tc(VII)O_4^-$ plumes at Hanford reside in the Ringold formation. A clay-rich saprolite was obtained from the Field Research Center (FRC) background site located in the West Bear Creek Valley on the Oak Ridge Site in eastern Tennessee. This material is referred to as FRC saprolite. A nearby TcO_4^- and UO_2^{2+} plume exists in these same sediment types. An Fe(III)-oxide containing subsurface sediment was also collected from a Pleistocene-age coastal plain deposit near Eatontown, N.J., approximately 3 m below land surface (Zachara et al., 1998). This material is referred to as Eatontown hematite.

The subsurface materials were air-dried and passed through a 2-mm sieve before use. Surface area was measured by multipoint Brunauer-Emmett-Teller analyses. Extractable oxides were determined using three methods as previously described (Zachara et al., 1998). These methods included hydroxylamine hydrochloride for amorphous Fe(III) oxyhydroxides and reducible Mn(III/IV) oxides, dithionite-citrate-bicarbonate (DCB) for extraction of reducible Fe(III) oxides, and acidified ammonium oxalate for amorphous aluminosilicates as well as poorly crystalline Fe(III) oxides.

2.2. Bacteria and Media

S. putrefaciens strain CN32 was provided courtesy of Dr. David Boone (Subsurface Microbial Culture Collection, Portland State University, Portland, OR). Strain CN32 was isolated from a subsurface core sample (250 m beneath the surface) from the Morrison Formation in northwestern New Mexico (Fredrickson et al., 1998). For these experiments, CN32 was routinely cultured aerobically in tryptic soy broth (TSB), 30 g L^{-1} (Difco Laboratories, Detroit, MI), and stock cultures were maintained by freezing in 40% glycerol at −80°C. For batch experiments, CN32 cells were harvested from TSB cultures at mid to late log phase by centrifugation, washed twice with 30 mM PIPES buffer and once with pH 7 bicarbonate buffer to remove residual medium. The cells were then suspended in bicarbonate buffer and purged with O_2-free N_2. Washed cells were added to obtain a final concentration of $2–4 \times 10^8$ cells mL^{-1}.

Biogenic $TcO_2 \cdot nH_2O_{(s)}$ was generated by incubating 1 mM $NH_4Tc(VII)O_4$ (Amersham Life Sciences Products, Arlington Heights, IL) in anaerobic 10-mM, pH 7 PIPES buffer with *S. putrefaciens* CN32 at $\sim 3 \times 10^8$ cells mL^{-1}. The culture volume was 80 mL in a 160-mL serum bottle, and 80 cc^3 of H_2 was added as an electron donor. Serum bottles were incubated at 35°C with periodic manual shaking for ~24 h. After incubation, solids were allowed to settle and were further concentrated by centrifugation. The concentrated solids were incubated with a 10% NaOH solution that had been purged with N_2 to remove O_2 and were shaken 50 rpm for 3 d at 30°C. The solids were once again concentrated by centrifugation and washed 3× with 0.1 mol/L anaerobic sodium perchlorate. After three washes the solids were resuspended in the anaerobic perchlorate solution, sonicated for 60 min, and maintained under anaerobic conditions until used.

2.3. Bacterial Reduction Experiments

Bioreduced sediments (in triplicate) were generated by incubating 0.5 or 1 g sediment in 10 mL of 30 mM pH 7 bicarbonate buffer with $7–9 \times 10^7$ cells mL^{-1} *S. putrefaciens* CN32 and 10 mM sodium lactate as electron donor, in a N_2:CO_2 (80:20) headspace, at 30°C with shaking @ 25 rpm. At select time points, bioreduced sediments were pasteurized by heating at 80°C for 1 h and then frozen at −20°C until used. Viable cells of CN32 could not be detected by growth on TSB agar plates after pasteurization.

The concentrations of Fe and Mn in aqueous filtrates (0.2 μm) and 0.5 N HCl extracts (1 h, agitated at 25 rpm) were measured by inductively coupled plasma atomic emission spectroscopy, and Fe(II) was measured by the ferrozine assay. Tc was measured by liquid scintillation counting. All sample manipulations were conducted using strictly anaerobic techniques, including the use of an anaerobic glove box (Forma Scientific, Marietta, OH).

2.4. Tc(VII) Reduction Experiments

Unreduced and bioreduced subsurface materials were washed with a bicarbonate buffer/electrolyte solution, and spiked with $NH_4Tc(VII)O_4$ to yield an approximate concentration of 20 mM that was quantified at experiment initiation. The bioreduced samples were studied both without and with pasteurization to inactivate CN32. The Tc(VII)-spiked samples were agitated and equilibrated at 25°C and sampled over time to assess whether Tc(VII) was reduced and, if so, to measure the rate of reaction. Removed aqueous samples were filtered (<0.2 μm) and counted to determine the Tc(VII) concentration.

2.5. Mössbauer Spectroscopy

Suspended solids were filtered and washed with acetone, then random-orientation absorbers were prepared by mixing 100–200 mg of the dried sample with petroleum jelly. The samples were mounted in a 1.3 cm I.D. Cu holder, in which excess sample space was filled with petroleum jelly, then sealed with clear tape. Bioreduced samples were handled under an anaerobic atmosphere. Spectra were collected at room temperature (RT) and liquid nitrogen temperature (77°K) using a ~50 mCi (1.85 GBq) (initial strength) ^{57}Co/Rh single-line thin source. The velocity transducer (MVT-1000; WissEL) was operated in constant-acceleration mode (23 Hz, ±10 mm/s). Data were acquired on 1024 channels and then folded to 512 channels to give a flat background and a zero-velocity position corresponding to the center shift (CS or δ) of a metallic-Fe foil at room temperature. Calibration spectra were obtained with a 20-μm-thick α-Fe foil (Amersham, England) placed in exactly the same position as the samples to minimize error associated with changes in geometry. The transmitted radiation was recorded with an Ar-Kr proportional counter. The unfolded spectra obtained were folded and evaluated with the Recoil program (University of Ottawa, Canada) using a Voigt-based hyperfine parameter distribution method. The recoil factor (f-factor) was assumed to be identical for all the phases. Under this assumption, the spectral areas, expressed as a percentage, reflect relative abundance of various phases.

2.6. X-ray Adsorption Near Edge Spectra (XANES) and X-ray Microprobe Analyses

After reaction, the residual solids were isolated by filtration under anoxic conditions, resin-embedded, and cut/milled into ca. 100-μm thin sections, mounted on fused quartz slides. Thin sections of pristine, bioreduced, and bioreduced/Tc(VII) reacted sediments were analyzed by scanning electron microscopy (SEM) at Pacific Northwest National Laboratory, and by X-ray microspectroscopy (XMP) at the PNC-CAT beamline at the Advanced Photon Source at Argonne National Laboratory. At the PNC-CAT, the primary X-ray beam was focused using Kirkpatrick-Baez mirrors to a 6–7-μm diameter on the sample surface, and characteristic X-ray fluorescence was detected using energy-dispersive and wavelength dispersive spectrometers. The sample was

Table 1. Sediment properties.

	FRC saprolite	Ringold 6–6/6–7	Eatontown hematite
NH_2OH-HCl (μmol/g)			
Mn	33.2	171	<0.02
Fe	44.4	18.4	17.5
Al	80.0	17.5	0.60
Ammonium-oxalate (μmol/g)			
Mn	30.5	200	<0.02
Fe	41.3	35.3	2.40
Al	34.9	11.0	1.11
DCB (μmol/g)			
Mn	35.7	198	<0.07
Fe	269	1371	366
Al	58.5	164	17.0
X-ray fluorescence (μmol/g)			
Mn	41.7	235	0.61
Fe	820	1399	495
CEC (meq/100 g)	11.6	4.6	0.073
Surface area (m^2/g)	32.2	21.9	3.1
Oxide Fe(III) (%)[a]	32	98	74
Silicate [Fe(III) + FeII)][b]	68	2	26

[a] Percent of total Fe.
[b] Percent of total Fe.

oriented in a precision-translation stage at 45° to the X-ray beam, and the detectors were oriented normal to the beam. Elemental maps were obtained for Tc, Fe, and Mn by monitoring their K_α fluorescence lines. Some of the samples (the FRC sediment primarily) contained Zr particles (e.g., zircon), giving strong fluorescence that interfered with the Tc signals. For these samples, the Zr channel was also recorded to allow the actual Tc signal to be identified. The detection limit for all elements was less than 1 mg kg^{-1}, equivalent to approximately 10^9 atoms within the beam "spot." Fluorescence X-ray intensities, provided in the figures in false color, were normalized to the ion chamber current generated by the primary X-ray beam at a flux of $\sim 5 \times 10^{11}$ ph s^{-1}. These intensities were not compensated for differences in detection efficiency, which was estimated to be ~5–6 times higher for Tc than for Fe or Mn. SEM and XMP images were superimposed using Adobe PhotoShop.

X-ray absorption spectra were collected on Tc-containing regions of the thin section after the spatial distribution of Tc had been mapped. The X-ray beam was placed on Tc-containing regions and the incident energy was scanned while monitoring the X-ray fluorescence. A Si(111) double crystal monochromator was used with an energy resolution ($\Delta E/E$) of $\sim 1.4 \times 10^{-4}$. For the Tc edge at 21.044 keV, Mo foil was used to calibrate the beam energy, using the encoder-equipped monochromator drive. For the Mn and Fe edges, Fe foil was used to check the monochromator energy calibration. For the Fe edges, the high concentration in the samples caused some distortion of the signals due to self-absorption, but the Fe valence could be determined and no corrections were attempted. For comparison, various Mn and Fe standards were measured in transmission mode using fine powders rubbed onto tape.

3. RESULTS

3.1. Mineralogic and Chemical Characteristics of Sediments

All three sediments contained significant amounts of total Fe, and Fe(III) in the form of extractable Fe(III) oxides (Table 1). Most of the extractable Fe(III) oxides were crystalline (>75%) as shown by the higher amounts of DCB-Fe(III) over that removed by the other extractions. By comparing the total Fe measured by X-ray fluorescence with that extracted by DCB, it was found that the sediments varied in their distribution of silicate Fe and extractable Fe(III) (Table 1). Iron present in the Ringold sediment existed almost entirely (98%) as an extractable Fe(III) oxide, whereas the predominant form of Fe in the FRC sediment was silicate Fe (68%). The Eatontown sediment exhibited intermediate behavior. Extractable Mn was highest in the Ringold sediment (≈200 μmol g^{-1}), followed by the FRC sediment (≈35 μmol g^{-1}). The Eatontown sediment contained low levels of Mn.

The sediments varied in their mineralogic character and texture (Table 2), although each contained either goethite or hematite as the primary Fe(III) oxide. Both the Ringold and Eatontown sediments were sand-textured materials resulting from fluvial deposition (see Zachara et al., 1995 for previous studies on the Ringold sediment and Zachara et al., 1998 for previous studies on the Eatontown sediment). Sand grain surfaces (primarily quartz and feldspars) in these materials were extensively coated with discrete oxide precipitates, Fe(III) and Mn(III/IV) oxides in the Ringold sediment and Fe(III) oxides only in the Eatontown. The FRC sediment was markedly different from the other two. The sample studied was obtained by compositing several distinct strata of a shale-limestone saprolite. The FRC composite sediment consisted of sand- and silt-sized aggregates of fine grained material including quartz, mica, vermiculite, and illite.

The Fe(III) oxide fraction in the Ringold and FRC sediments showed morphologic similarity (Fig. 1) despite their different pH and environmental origin. Radiant goethite crystallites, aggregates of 100–200 nm acicular crystallites, and discrete goethite laths in a matrix of illite were common to the FRC sediment (Fig. 1a). Smaller radiant goethite crystallites and discrete laths were observed in the Ringold sediment along with massive lath aggregates (Fig. 1b). Globular hematite precipitates of indistinct morphology with approximate size of 1 μm were common to the Eatontown sediment (Fig. 1c). Energy-dispersive spectrometry analysis of both the Eatontown hematite (Zachara et al., 1998) and the FRC goethite defined the presence of Al substitution, while similar analysis for

Table 2. Mineral character of subsurface sediments.

	Fe(III) oxide	Mn(III/IV) oxide	Matrix	Texture
FRC	<100 nm Al-goethite with acicular habit	Unknown, <50 nm	Quartz, illite, mica, and vermiculite	Sand- and silt-sized aggregates of finer grained material
Ringold	<100 nm Si-containing goethite with acicular habit	Todorokite	Quartz, mica, plagioclase	Medium sand with extensive particle coatings of Fe(III) and Mn(III/IV) oxides
Eatontown	Micron-sized, globular hematite	None	Quartz, feldspar	Medium sand with grain mottling by precipitated hematite

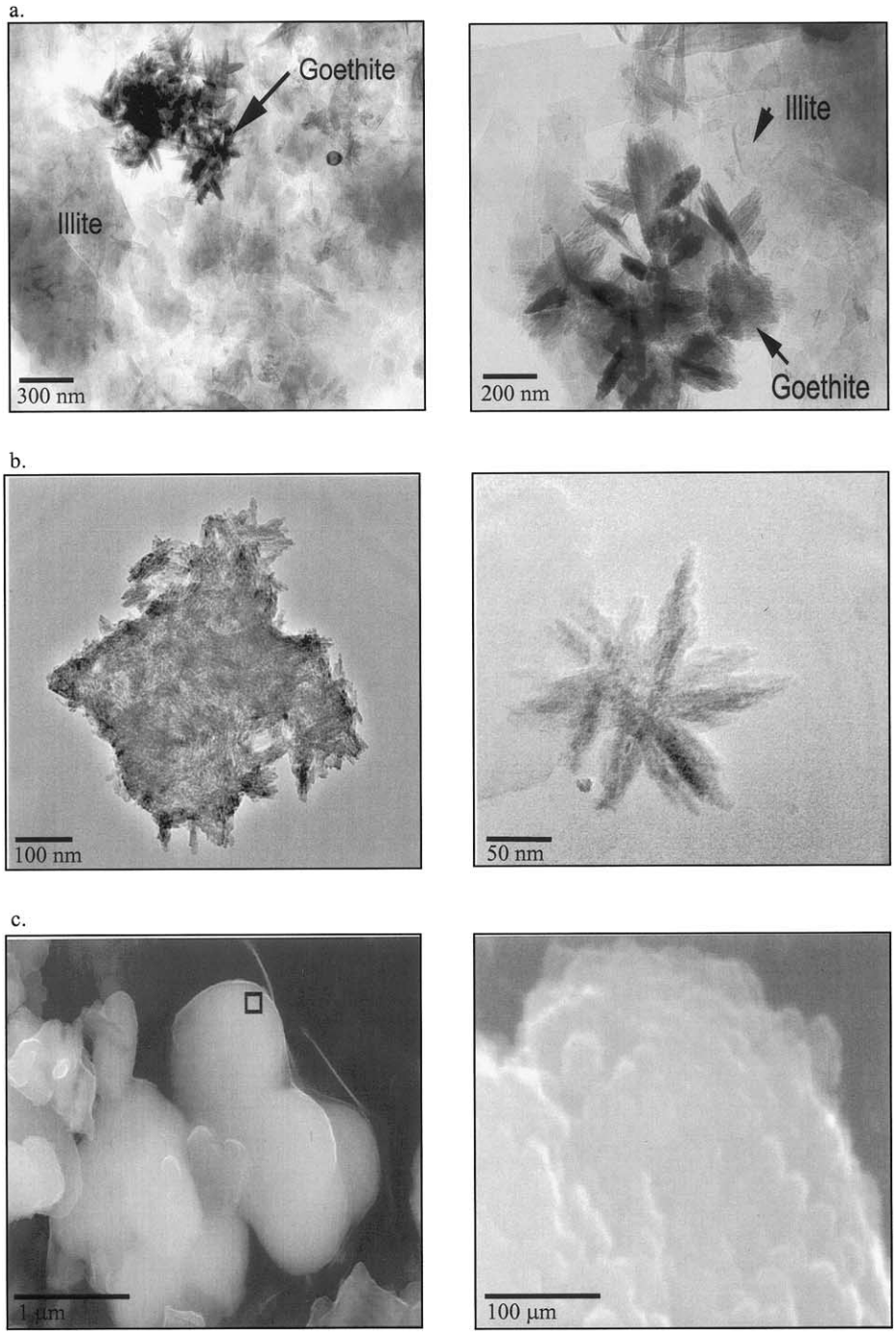

Fig. 1. Scanning electron micrographs of Fe(III) oxides in the studied sediments (a) FRC, (b) Ringold, (c) Eatontown.

Ringold sediment showed the presence of co-reacted Si with the Fe(III) oxide (Zachara et al., 1995). Mn(III/IV) oxides in the FRC sediment were difficult to observe, isolate, and identify but appeared to exist as discrete, <50 nm precipitates of undefined mineralogy. In contrast, Mn(III/IV) oxides in the Ringold sediment (todorokite) were 200–500 nm in size and exhibited well-defined tabular morphology consistent with phyllomanganates.

3.2. Bioreduction of Sediments

The microbial reduction of the FRC saprolite was evident at the first time point (5 d) by a significant increase in the concentration of total Mn extractable in 0.5 N HCl (Fig. 2). For comparison, the concentration of Mn in a 0.5 N HCl extract of unreduced FRC saprolite was 0.46 mM and in uninoculated controls with 10 mM lactate the concentration of HCl-extract-

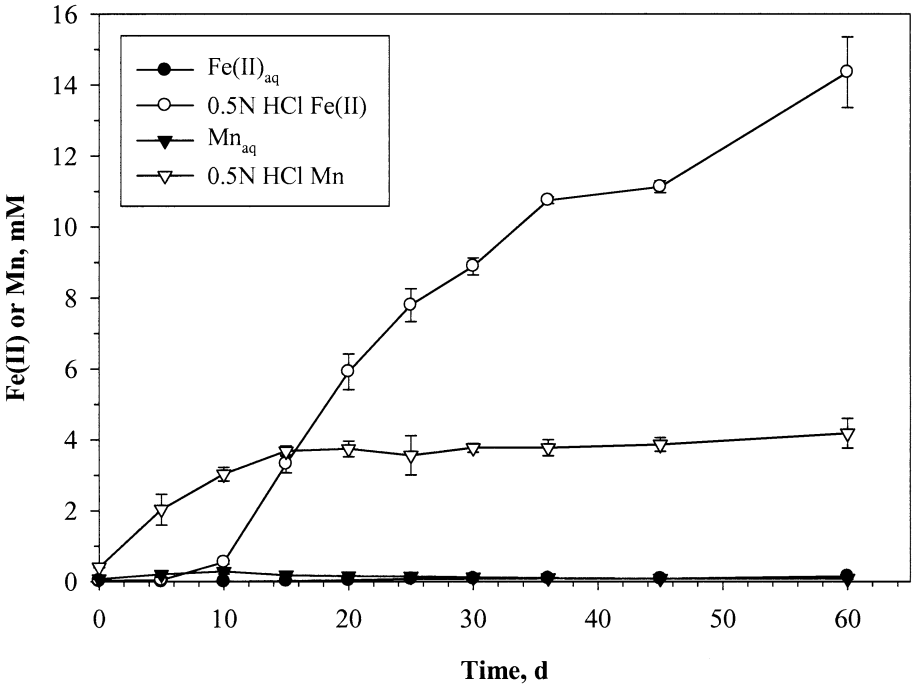

Fig. 2. Concentrations of aqueous (0.2 μm-filtered) and 0.5 N HCl-extractable Mn and Fe(II) during reduction of FRC saprolite by *S. putrefaciens* CN32 in 30 mM $NaHCO_3$, pH 7 buffer with 10 mM Na lactate.

able Mn was only 0.42 ($\pm$0.20) mM after 25 d incubation. It was assumed that the increase in the acid-extractable Mn was due to the reduction of Mn(III/IV) to Mn(II) by CN32, although microbial processes contributing to an increased susceptibility of Mn(III/IV) to acid extraction cannot be ruled out. Nonetheless, previous studies have demonstrated that CN32 is capable of reducing synthetic Mn oxides leading, in some cases, to the precipitation of $MnCO_3$ (rhodochrosite) (Fredrickson et al., 2002).

There was little indication of net Fe(III) reduction, as evidenced by HCl-extractable Fe(II) until essentially all of the Mn extractable by NH_2OH-HCl (Table 1) had been converted to a form extractable by 0.5 N HCl, presumably by microbial reduction. This occurred between 10 and 14 d after inoculation with CN32 (Fig. 2). Fe(III) reduction continued at a relatively steady rate up to 60 d at which time the incubations were terminated. At this time, the amount of Fe(III) reduced represented 17.6% of the total Fe (Table 1, X-ray fluorescence) and 53.5% of the DCB-extractable fraction. The concentrations of aqueous Fe(II) and Mn were at or near detection limits (Fig. 2) during the entire experiment indicating that essentially all of the bioreduced Fe and Mn was associated with the solid phase.

^{57}Fe Mössbauer spectroscopy is a relatively sensitive method for characterizing the Fe phases in sediments before and after microbial reduction (Kukkadapu et al., 2001; Zachara et al., 2004) as well as with synthetic Fe oxides subjected to microbial reduction (Fredrickson et al., 2001; Zachara et al., 2002), although it does have its limitations. In contrast to X-ray diffraction, Mössbauer provides information on compounds that do not exhibit long-range structural order (poorly crystalline materials) (Bancroft, 1973). The central doublet (-1 mm/s) and (apparent) singlet (high field component of Fe(II) doublet 2.5 mm/s) of the 77°K Mössbauer spectra of the unreduced FRC saprolite (Fig. 3, solid line) represent Fe(III) and Fe(II) in a phyllosilicate environment. The sextet resulted from small particle or Al substituted goethite (α-FeOOH) (e.g., Fig. 1a). The goethite spectral area (M1, Fig. 3b) decreased from 36% to 29% and the Fe(II) spectral area increased from 13% to 23% during bioreduction (Fig. 3b,c). Goethite bioreduction was the apparent source of Fe(II). Unfortunately, these 77°K Mössbauer analyses, alone, did not allow identification of the specific form of biogenic Fe(II) that was formed. The high-energy component of the paramagnetic Fe(II) Mössbauer doublet for phyllosilicate, carbonate, and green rust structural environments all fall in close proximity to 2.3–2.6 mm/s where the biogenic Fe(II) signal was observed.

In the Ringold 6-6/6-7 sediment, the high concentration of Mn(III/IV) appeared to buffer the Fe(III) oxide fraction against reduction by CN32. After 43 d there was a negligible increase in the concentration of 0.5 N HCl-extractable Fe(II), but the concentration of weak acid extractable Mn had increased to 16.9 mM (Fig. 4a). This amount of Mn represents 71.9% of the total Mn, as determined by X-ray fluorescence, and essentially 100% of the NH_2OH-HCl extractable Mn (Table 1). In uninoculated controls with 10 mM lactate, the concentration of 0.5 N HCl extractable Mn was only 1.06 (0.38) mM after incubation for 25 d. As with the FRC saprolite, the concentrations of aqueous Fe(II) and Mn were near or below detection during the entire course of the experiment (data not shown). In an effort to facilitate the bioreduction of Fe(III) in the Ringold sediment, a second experiment was conducted with a lower solids concentration (0.5 g) than the first experiment (1.0 g). Using this approach, the 0.5 N HCl extractable Mn and Fe(II) were 11.1

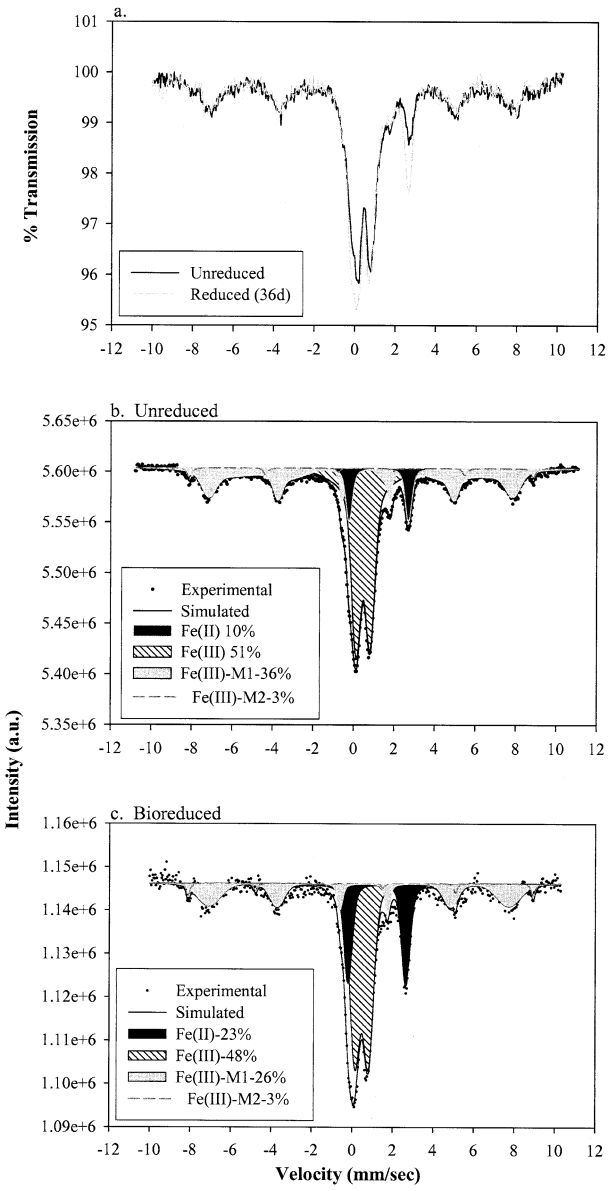

Fig. 3. Mössbauer spectra (77°K) of unreduced FRC saprolite and material bioreduced by *S. putrefaciens* CN32 pH 7, 30 mM $NaHCO_3$ buffer (a) and 77°K spectra (experimental and simulated) of the unreduced (b) and bioreduced (c) sediment.

and 4.0 mM, respectively, after incubation with CN32 for 60 d (Fig. 4b).

The Mn oxides in the unreduced Ringold sediment were predominantly a todorokite-like phase as determined by X-ray diffraction and transmission electron microscopy (data not shown). Mössbauer analysis at RT and 77°K revealed that small particle goethite (sextet–magnetic) and lepidocrocite (doublet–paramagnetic) dominated the Fe(III) oxide fraction in the unreduced sediment (Fig. 5a). The Mössbauer spectra (77°K) of the 60 d bioreduced Ringold sediment (0.5 g in 15 mL) revealed that approximately 4% of the ^{57}Fe signal was due to Fe(II), at −0.5 and +2.5 mm/s. These peak energies were roughly consistent with those of siderite (Ono and Ito, 1964). The generation of Fe(II) could be attributed to small decreases in both lepidocrocite and goethite (Fig. 5c). The Mössbauer spectral area for Fe(II) was in close agreement with the Fe(II) extracted by 0.5 N HCl (4.8 mM or 5% of the total Fe). The bulk XANES spectra for the bioreduced Ringold sediments (data not shown) indicated a progressive fractional reduction of Mn(III/IV) over the first 21 d after which the Mn valence did not change appreciably. The average final valence state for Mn was above 2. MicroXANES measurements of Ringold sediment incubated with CN32 for 43 d showed that the Mn valence was variable at the 10–100 μm scale.

The Eatontown sediment enriched in hematite was included in this study for comparative purposes as it, in contrast to the FRC saprolite and Ringold sediment, contained little or no Mn(III/IV) oxide (Table 1). Room temperature Mössbauer spectra of unreduced Eatontown hematite (Fig. 6) revealed the presence of highly crystalline hematite (sextets, ~83% of Fe_{TOT}). The hyperfine magnetic field of the sedimentary hematite was less than for a crystalline hematite without any foreign metal ion substitution, implying Al(III) substitution that was confirmed by energy-dispersive spectrometry analysis. Ap-

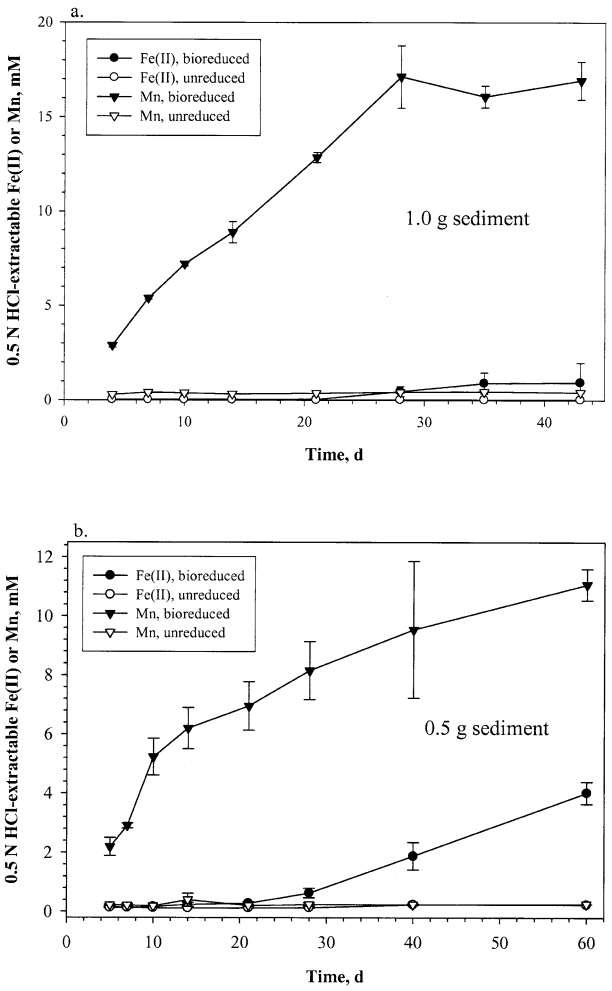

Fig. 4. Concentrations of aqueous (0.2 μm-filtered) and 0.5 N HCl-extractable Mn and Fe(II) during reduction of 1.0 g/tube (a) and 0.5 g/tube (b) Ringold Formation sediment by *S. putrefaciens* CN32 in 30 mM $NaHCO_3$, pH 7 buffer with 10 mM Na lactate.

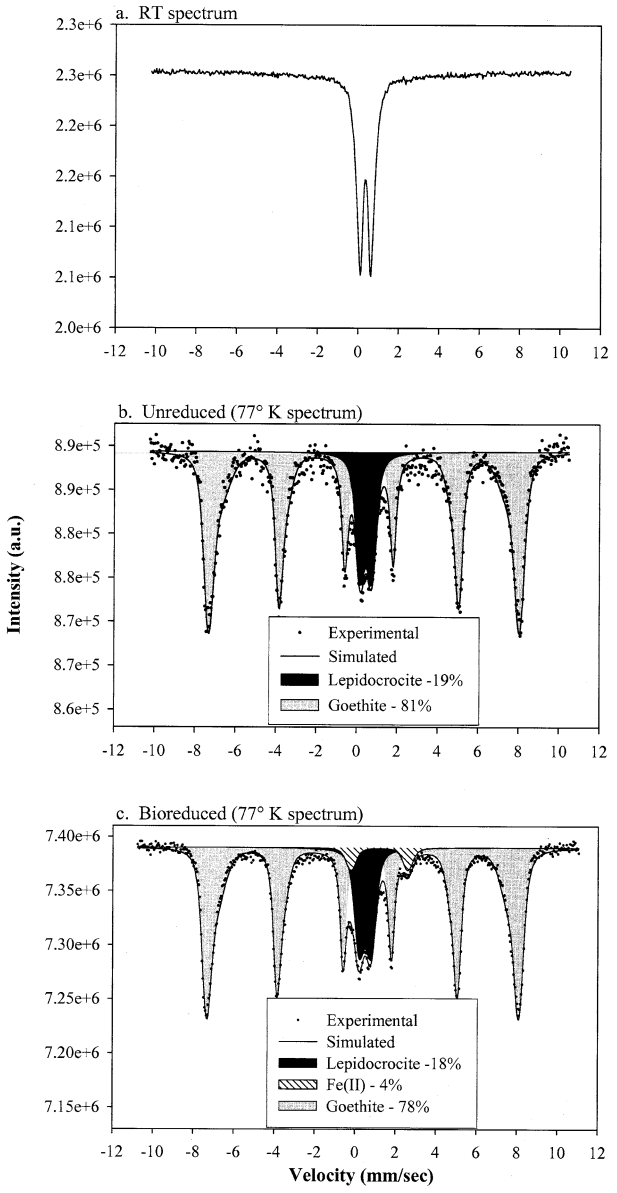

Fig. 5. Mössbauer spectrum (RT) of unreduced Ringold sediment (a) 77°K spectrum of the unreduced sediment and (b) 60 d bioreduced by *S. putrefaciens* CN32 in pH 7, 30 mM $NaHCO_3$ buffer (c).

proximately 17% of the total Fe(III) was associated with the central doublet of the Mössbauer spectrum that represents Fe(III) in a crystalline silicate environment (Zachara et al., 2004).

Because the Fe(III) in the Eatontown sediment was previously demonstrated to be partially reducible by CN32 (Zachara et al., 1998), an intensively sampled reduction experiment was not conducted. Rather, bioreduced sediments were pasteurized at select time points and frozen (−20°C) until used in experiments investigating the abiotic reduction of Tc(VII). The extent of Fe(III) reduction in these samples was determined at the time of pasteurization. The Mössbauer spectrum of the 26 d bioreduced Eatontown sediment showed little or no discernable change from the pristine sediment (Fig. 6b).

3.3. Abiotic Interactions of $Tc(VII)O_4^-$ and $TcO_2 \cdot nH_2O$ With Bioreduced and Unreduced Sediments

Tc(VII), as ammonium pertechnetate, and biogenic $TcO_2 \cdot nH_2O$ were added to FRC sediment that had been incubated for 5 d with CN32 and then pasteurized, and to unreduced anaerobic sediment suspensions. In cell suspensions with CN32 cells only, pasteurization (heating to 80°C for 1 h) eliminated Tc(VII) reduction for up to 8 d and was assumed to be equally effective in eliminating biologic reduction in the cell-sediment suspensions. In the pasteurized bioreduced suspensions there was a modest loss of TcO_4^- from solution over the 305-d incubation, but the variation was quite high while there was little or no loss from the unreduced control sediment (Fig. 7a). Over the same time period there was significant but incomplete solubilization of Tc from $TcO_2 \cdot nH_2O_{(s)}$ in both the 5-d bioreduced and unreduced sediment, although the amount of Tc solubilized was slightly higher in the unreduced material (Fig. 7a). The increase in $Tc_{(aq)}$ likely resulted from the oxidation of $TcO_2 \cdot nH_2O_{(s)}$ by sediment-associated Mn(III/IV) oxides in the unreduced and partially reduced materials. After 5 d of incubation with CN32, approximately 30% of the NH_2OH-HCl extractable Mn was extractable by 0.5 N HCl, presumably due to microbial Mn reduction, likely accounting for the slightly slower oxidation of $TcO_2 \cdot nH_2O_{(s)}$ compared to the unreduced solids.

The abiotic reduction of TcO_4^- was investigated in the FRC sediment that had been incubated with *S. putrefaciens* CN32 for increasing lengths of time. The incubations yielded a series of bioreduced sediments with increasing biogenic Fe(II) concentrations (e.g., Fig. 2). In sediment that had been reduced for 17 d, >99% of the initial TcO_4^- was reduced to an insoluble phase in <2 d, whereas in the 25-d bioreduced sediment, >99% of the Tc(VII) was reduced within 15 h (Fig. 7b). In comparison, the reduction of TcO_4^- in 36-d bioreduced FRC sediment was nearly instantaneous with soluble concentrations of Tc decreasing to below detection within minutes after addition to the pasteurized suspensions (Fig. 7c). In contrast to the 5-d bioreduced sediment, biogenic $TcO_2 \cdot nH_2O_{(s)}$ added to pasteurized 36-d bioreduced sediment was not solubilized over a 42-d period. Over this same time period, >75% of the $TcO_2 \cdot nH_2O_{(s)}$ added to the unreduced but anoxic control sediment was converted to a soluble species (Fig. 7c). After 12 d incubation with CN32, essentially all of the NH_2OH-HCl extractable Mn had been reduced.

Ringold sediments (0.5 g) were reduced for 21, 28, 40, and 60 d and then investigated for their capacity to reduce TcO_4^- in a manner identical to that for the bioreduced FRC as described above. Similar to the FRC saprolite, the more extensive the bioreduction of Fe(III), the more rapid and extensive the reduction of TcO_4^- (Fig. 8). The standard errors for the three replicates from the 28-d and 40-d bioreduced samples were high, reflecting the considerable variation in the extent of Fe(III) bioreduction at some of the intermediate time points (Fig. 4). Sometimes it was observed that one of the three replicates showed no TcO_4^- reduction, while the other two did. The reason for this variation is unclear but it was specific to the Ringold sediment and may have been due to a greater degree of heterogeneity in particle size and distribution of Fe(III) and Mn(III/IV) phases. After bioreduction for 60 d the variation in

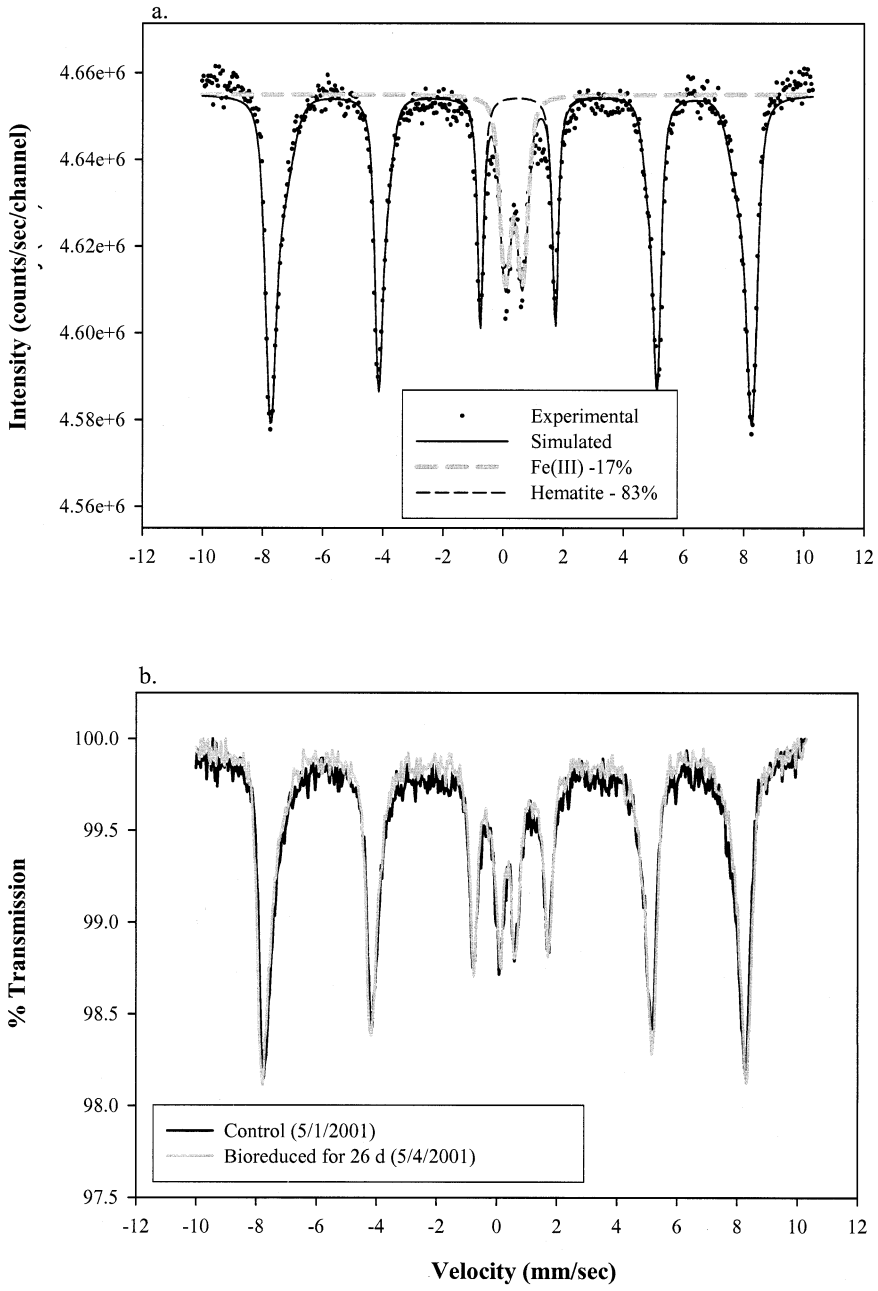

Fig. 6. Experimental and simulated Mössbauer spectra (RT) for the unreduced Eatontown sediment (a) and overlay of Mössbauer spectrum (RT) for the Eatontown sediment after 26 d incubation with CN32 in 30 mM $NaHCO_3$ pH 7 buffer with 10 mM lactate (b).

Fe(III) reduction was much lower and these samples exhibited a rapid and extensive capacity for TcO_4^- reduction (Figs. 4 and 8).

Bioreduced Eatontown hematite sediment was also very effective at reducing TcO_4^- as ~95% of the initial Tc(VII) added was removed from solution in <48 h in sediment reduced for only 2 d (Fig. 9). Similar to the results with the FRC and Ringold materials, the longer the period of bioreduction by CN32 and the higher the concentration of solid phase–associated Fe(II) (0.5 N HCl extractable), the more rapid and extensive was the removal of TcO_4^- from solution. The capacity of the Eatontown hematite to reduce Tc(VII), even after a relatively short reduction period, was due, in part, to the absence of Mn(III/IV) oxides that buffered redox potential in the other two sediments. The Eatontown hematite sediment that was incubated with CN32 for only 2 d with a 0.5 N HCl-extractable Fe(II) content of 0.27 mM, reduced TcO_4^- at a rate (Fig. 9) comparable to the FRC material incubated for 17 d with 5.73 mM HCl-extractable Fe(II) (Fig. 7b).

3.4. X-ray Absorption Spectroscopy Analyses

The spatial distribution of Tc associated with mineral aggregates in the FRC saprolite and lithic fragments in the Ringold

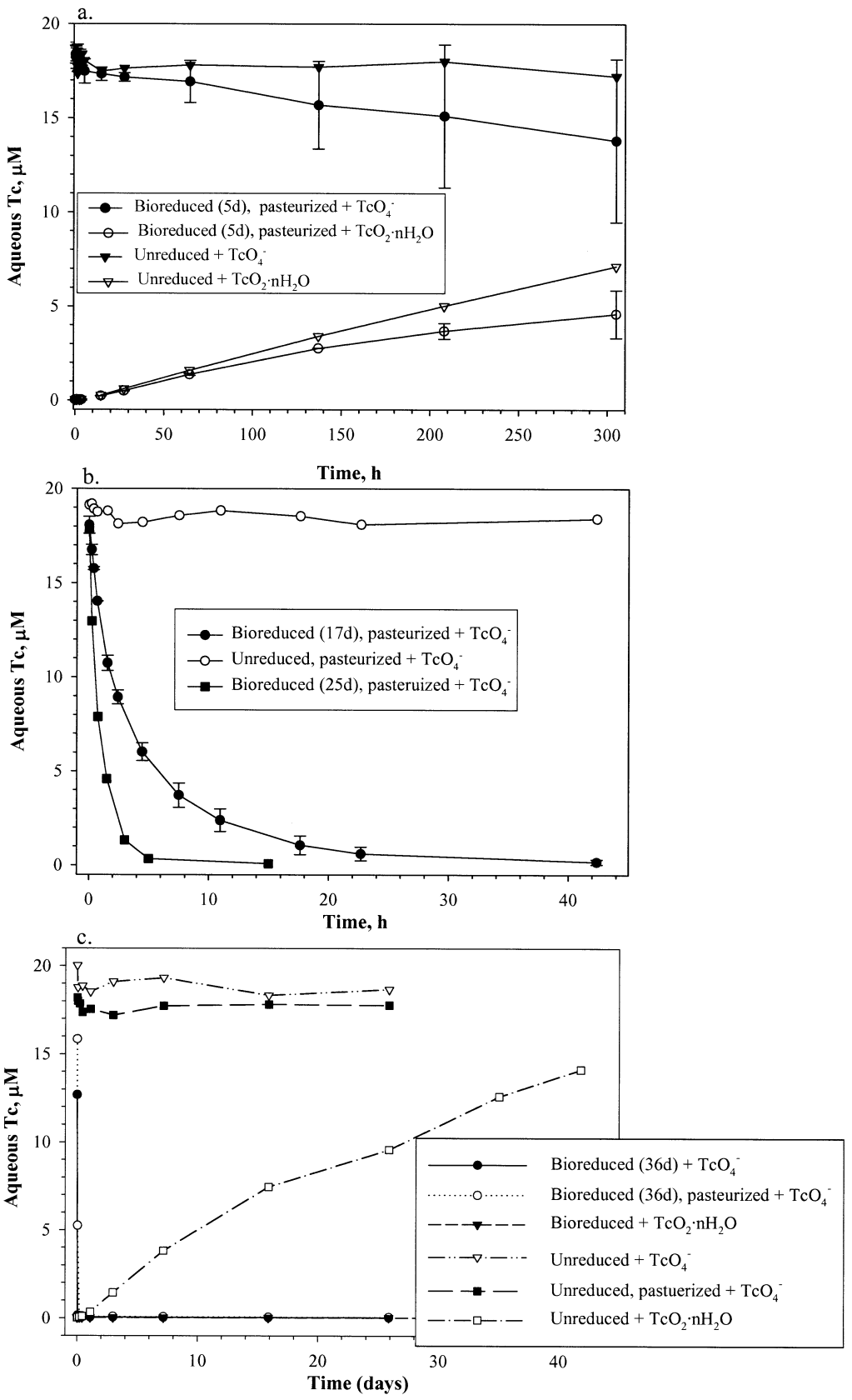

Fig. 7. Tc solubility in FRC saprolite biologically reduced in 30 mM $NaHCO_3$ pH 7 buffer with 10 mM Na lactate for various lengths of time and then pasteurized at 80°C for 1 h. The initial 0.5 N HCl-extractable Fe(II) and Mn were 0.056 and 1.29 mM, respectively, for sediment bioreduced for 5 d. Pertechnetate was added as 20 μM $(NH_4)_1TcO_4$ and $TcO_2 \cdot nH_2O_{(s)}$ was added to 20 μmol Tc(IV) L^{-1}, and the concentrations of $Tc_{(aq)}$ were determined with time (a). The 0.5 N HCl-extractable Fe(II) and Mn were 5.73 ($\pm$0.13) and 3.46 ($\pm$0.26) mM, respectively, for 17 d and 7.80 ($\pm$0.47) and 3.57 ($\pm$0.55), respectively for 25 d (b). For the FRC saprolite bioreduced for 36 d, the 0.5 N HCl-extractable Fe(II) and Mn concentrations were 10.75 ($\pm$0.10) and 3.78 ($\pm$0.23) mM, respectively (c).

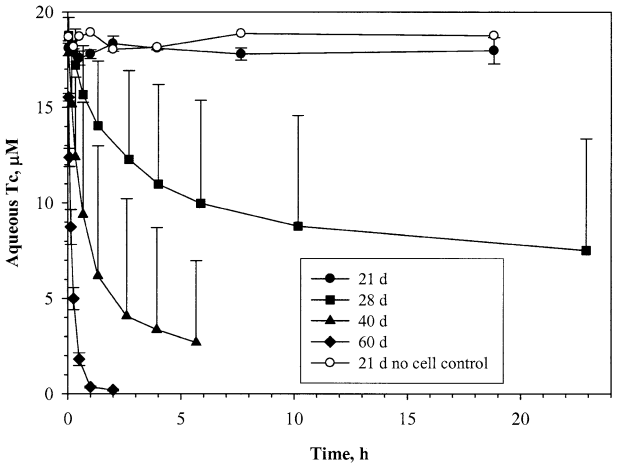

Fig. 8. Tc solubility in Ringold sediment biologically reduced in 30 mM $NaHCO_3$ pH 7 buffer with 10 mM Na lactate for various lengths of time and then pasteurized at 80°C for 1 h. Pertechnetate was added as 20 μM $(NH_4)_1TcO_4$ and $TcO_2 \cdot nH_2O_{(s)}$ was added to 20 μmol Tc(IV) L^{-1}, and the concentrations of $Tc_{(aq)}$ were determined with time. Only the + error bars were included for the sediments bioreduced for 28 and 40 d to minimize clutter.

subsurface materials indicated that the sediments were heterogeneous with respect to Tc(IV) localization and, presumably, sites of TcO_4^- reduction. The valence of Tc in all bioreduced sediments that were reacted with TcO_4^- was confirmed to be Tc(IV) by microXANES (Fig. 10). Overlaying the X-ray microprobe (XMP) elemental abundance maps on backscattered electron (BSE) images revealed qualitative relationships between Tc reduction sites, chemical composition, and mineralogy in the FRC (Fig. 11) and Ringold (Fig. 12) sediments. The FRC sediment contained mineral aggregates that could be separated into two petrographically distinct groups; the most pronounced distinction being the relative abundance of Fe within them (i.e., Fe-rich or Fe-poor [Fig. 11]). The FRC background sediment was a composite material, and the different aggregate types are believed to represent distinct strata in the shale-limestone saprolite that were combined in the composite. These aggregates exhibited some differences with respect to their apparent association with Tc(IV). Tc was preferentially localized to the relatively Fe-poor aggregates, or Fe-poor regions within individual aggregates. Although Fe(III) was too abundant overall to allow differential mapping of Fe(II) in these sediments, the variable Tc spatial distribution may be due to several factors. The Fe(III) in the Fe-poor aggregates may have been more available for microbial reduction than that in the Fe-rich regions, resulting in localized areas of solid phase–associated, reactive Fe(II). Alternatively, the Fe-poor regions and the phyllosilicates within them may exhibit higher sorptivity for Fe(II).

The Ringold sediment (Fig. 12) contained abundant coarse-grained fragments of silicate minerals including quartz, feldspar, and biotite. There were abundant grain-coating concretions of Fe and Mn oxides on these, and the biotites (Fig. 12) were significantly altered by weathering reactions to include copious interlaminar concretions of intergrown Fe(III)-Mn(III/IV) oxides (see BSE image in Fig. 12). The concretions were too fine-grained to distinguish discrete Fe(III) and Mn(IV) phases by XMP, and the proportional contents of these elements were variable. The distribution of Tc(IV) was again heterogeneous, but in a way that was distinct from the FRC sediment. Tc(IV) was concentrated in Fe-rich regions, partic-

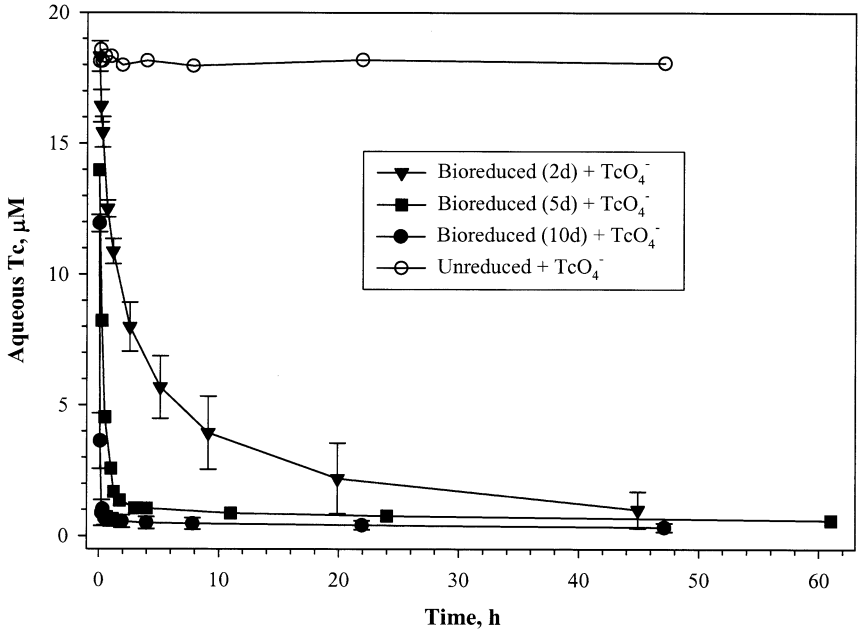

Fig. 9. Tc solubility in Eatontown hematite bioreduced by *S. putrefaciens* CN32 for 2, 5, and 10 d in 30 mM $NaHCO_3$ pH 7 buffer with 10 mM Na lactate followed by pasteurization. The 0.5 N HCl extractable Fe(II) concentrations were 0.03, 0.27 (±0.01), 0.53 (±0.02), and 1.07 (±0.08) mM for the unreduced control, 2-, 5-, and 10-d bioreduced sediment, respectively.

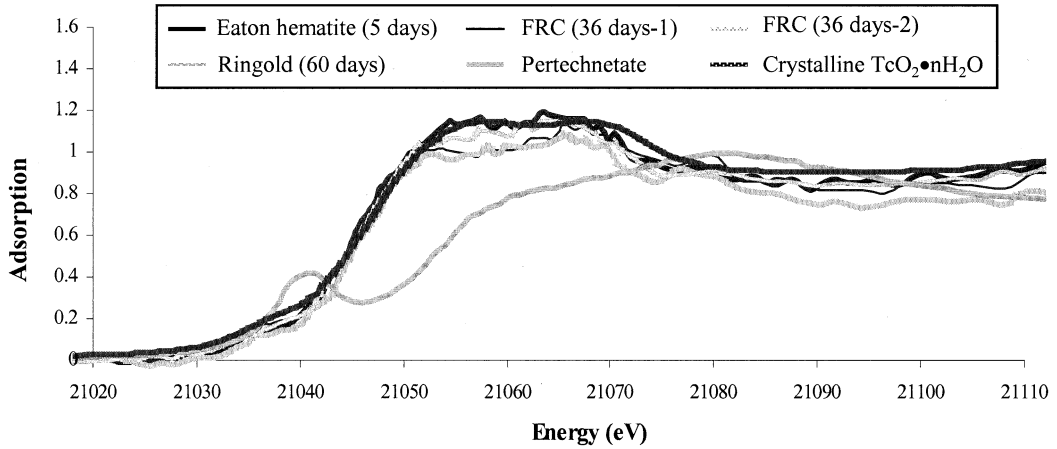

Fig. 10. X-ray adsorption near edge spectra (XANES) for pertechnetate [Tc(VII)], crystalline $TcO_2 \cdot nH_2O$ [Tc(IV)], and bioreduced Eatontown, FRC, and Ringold sediments with reacted TcO_4^-.

ularly on the surfaces of specific mineral grains and lithic fragments. With respect to biotite particles, however, Tc(IV) was concentrated on the rock fragment surfaces and *not* in the interlaminar spaces, where Fe and Mn oxides were abundant. This suggests that the Fe(III) in interlaminar spaces was less bioavailable and therefore less likely to contain Fe(II) that could, in turn, reduce TcO_4^-. This interpretation is consistent with the observation that some Mn(III/IV) persisted during

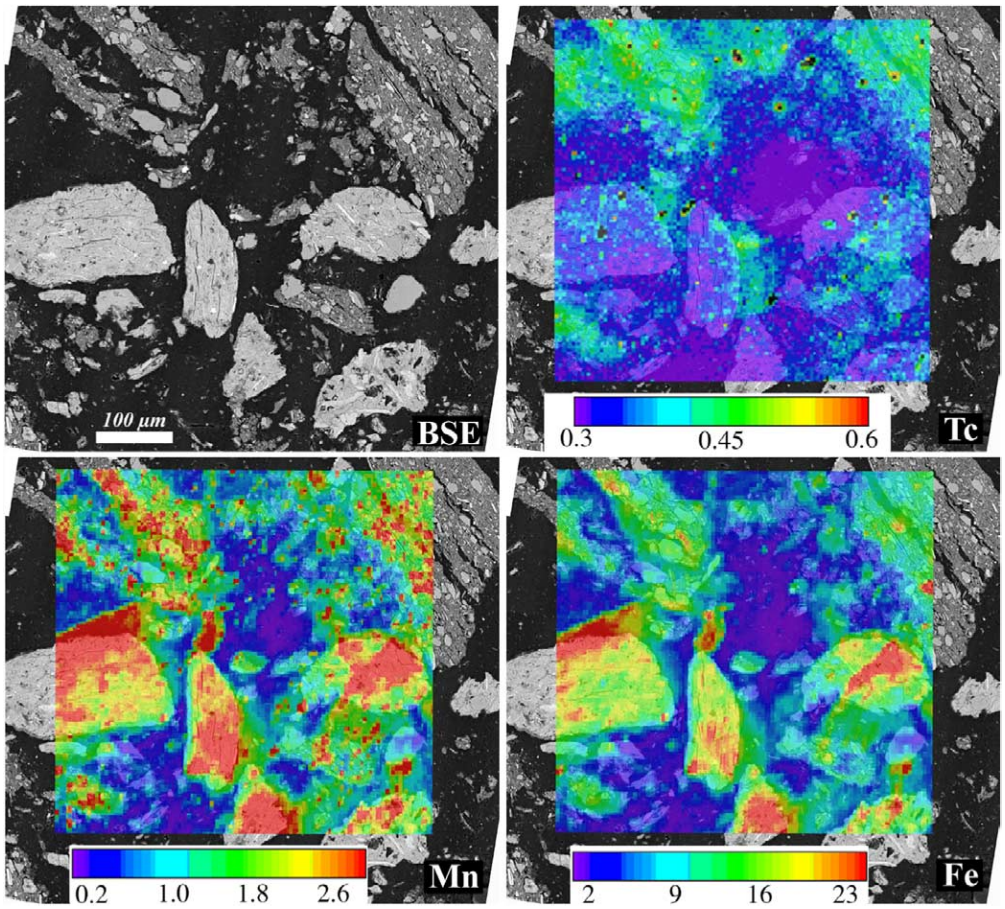

Fig. 11. X-ray microprobe false color elemental maps for Tc, Fe, and Mn, and SEM image of bioreduced FRC saprolite that was pasteurized and subsequently equilibrated with TcO_4^-. The intensities for characteristic fluorescence (scale bars) were normalized to the primary X-ray flux.

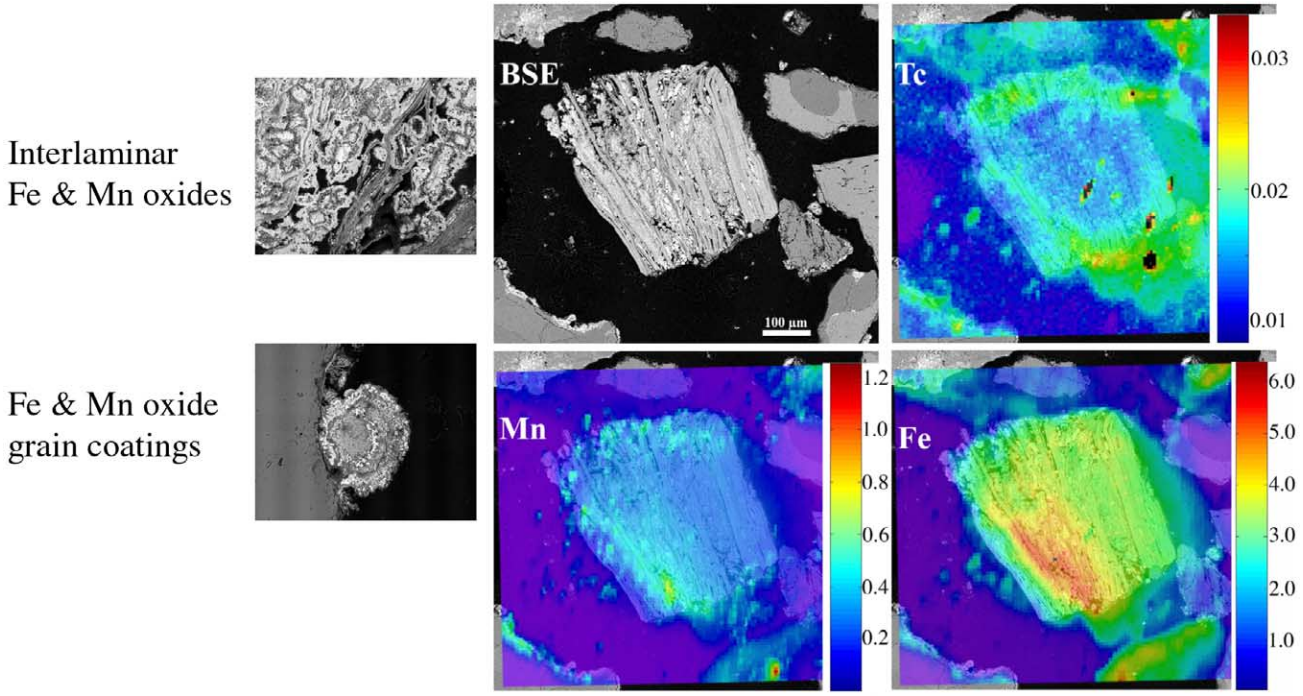

Fig. 12. X-ray microprobe false color elemental maps for Tc, Fe, and Mn, and SEM image of bioreduced Ringold sediment that was pasteurized and subsequently equilibrated with TcO_4^-. The intensities for characteristic fluorescence (scale bars) were proportioned to the primary X-ray flux.

bioreduction, probably as a result of its interlaminar residence and physical protection against reduction by *Shewanella*. The inability of this residual Mn(III/IV) to react with redox-sensitive species such as Fe(II) or Tc(IV) may also be due to this same physical protection mechanism, resulting in a global redox disequilibrium. The inexact spatial registry of Tc localization to the biotite surface (Fig. 12) results from the high energy of the APS synchrotron beam and the activation and fluorescence of Tc from deeper within the thin section.

4. DISCUSSION

4.1. Bioreduction of Mn(III/IV) and Fe(III)

The reduction of Mn(III,IV) and Fe(III) by *S. putrefaciens* CN32, as determined by the concentration of Mn and Fe(II) extracted by 0.5 N HCl, proceeded in a manner consistent with the thermodynamics of the redox couples of these metals. Little or no extractable Fe(II) appeared in either the FRC or Ringold material until essentially all of the NH_2OH-HCl extractable Mn was converted to a 0.5 N HCl extractable phase, presumably due to bioreduction. Investigations of microbial Fe(III) reduction in anaerobic sediments revealed that Mn(IV) retards net Fe(III) reduction, likely due to rapid heterogeneous oxidation of Fe(II) if and when produced (Lovley and Phillips, 1988; Myers and Nealson, 1988). Our results were consistent with this proposed mechanism of retardation of Fe(III) bioreduction as an increase in 0.5 N HCl extractable total Fe occurred before a net increase in Fe(II) (Fig. 4b). This is interpreted as an accumulation of a weak acid-soluble, poorly crystalline Fe(III) phase resulting from the rapid oxidation of biogenic Fe(II) by Mn(III/IV).

In the Ringold sediment (1 g experiment), nearly all of the 10 mM lactate should have been consumed during the reduction of the Mn, assuming all of the extractable Mn in the unreduced sediment was in the +4 oxidation state and that the theoretical stoichiometry for the oxidation of lactate coupled to the reduction of Mn(IV) by *S. putrefaciens* CN32 is as follows:

$$2MnO_2 + CH_3CHOHCOO^- + 3H^+ = 2Mn^{2+} + CH_3COO^- + HCO_3^- + 2H_2O \quad (1)$$

Lactate and acetate concentrations in the 1-g sediment-CN32 suspensions were 0.66 and 9.04 mM, respectively, confirming that nearly all of the initial 10 mM lactate had been consumed with near stoichiometric conversion to acetate. Previous experiments with CN32 investigating the reduction of ferrihydrite (Fredrickson et al., 1998) and U(VI) in goethite suspensions (Fredrickson et al., 2000) indicated that the actual stoichiometry of lactate consumption coupled to metal reduction by this bacterium is typically less, ~70% on average, of theoretical. Therefore, the lack of HCl extractable Fe(II) in the Ringold sediment after an extended incubation period was likely due to bacterial respiration becoming electron donor limited. This explanation was supported by the observation that decreasing the amount of Ringold sediment from 1 to 0.5 g (e.g., decreasing the concentration of reducible Mn by one-half) resulted in more extensive Fe(III) reduction to approximately 4 mM as extracted with 0.5 N HCl (Fig. 4b). Analyses of lactate and acetate concentrations in the 0.5-g sediment-CN32 suspensions were 2.98 and 5.83 mM, respectively, indicating that these suspensions had not yet become electron donor limited.

Table 3. First-order rate constants for TcO_4^- reduction in variably bioreduced subsurface materials.

Sediment	Bioreduction period (d)	1st order rate (h^{-1})	0.5 N HCl Fe(II) (mM)
FRC	5	1.00 (0.079) × 10^{-2}	0.056
	17	0.359 (0.024)	3.46 (0.26)
	25	0.823 (0.025)	7.80 (0.47)
	36	0.995 (0.016)	10.75 (0.10)
Ringold	21	no reduction	0.29 (0.05)
	28	0.133–0.425	0.63 (0.16)
	40	0.187–1.347	1.89 (0.46)
	60	4.45 (0.12)	4.02 (0.37)
Eatontown	2	0.481 (0.032)	0.27 (0.01)
	5	1.75 (0.083)	0.53 (0.02)
	10	6.98 (0.86)	1.07 (0.08)

4.2. Abiotic TcO_4 Reduction Is Facilitated by Biogenic Fe(II)

In the FRC saprolite, significant rates of TcO_4^- reduction were not evident until essentially all of the hydroxylamine-HCl extractable Mn fraction was converted to a weak acid-extractable phase, probably Mn(II), and net HCl-extractable Fe(II) accumulated (Figs. 2 and 7). In fact, the Mn oxide component of this material appeared to be an effective oxidant of biogenic $TcO_2 \cdot nH_2O_{(s)}$ (Fig. 7a,c). This result is consistent with our previous findings that synthetic Mn oxides (pyrolusite, bixbyite, and K^+-birnessite) were effective oxidants of biogenic $UO_{2(s)}$ (Fredrickson et al., 2002) and that Mn oxides, in general, are functional oxidants of organic compounds (Stone, 1987; Stone and Morgan, 1984), inorganic ions (Burdige and Nealson, 1986; Fendorf and Zasoski, 1992; Lovley and Phillips, 1988), and organometallic complexes (Gorby et al., 1998; Zachara et al., 1995). Soils and saprolite from the Oak Ridge site in eastern Tennessee (where the FRC composite sediment was obtained) are known to contain abundant Mn(III/IV) oxides resulting from the weathering of micas, carbonates, and shale. These phases are disseminated in many circumstances and have defied mineralogic identification by X-ray diffraction and other such techniques, implying amorphous or microcrystalline character (Lee et al., 1990; Phillips et al., 1998; Phillips et al., 1997).

It is interesting to note that in the FRC saprolite bioreduced for 5 d, TcO_4^- was slowly bioreduced, although the standard error of the mean was high and, in similarly reduced material, biogenic $TcO_2 \cdot nH_2O_{(s)}$ was slowly oxidized (Fig. 7a). This apparent contradiction can be explained by microscopic heterogeneities in the distribution of reactive Fe(II) and Mn(III/IV) oxides (Fig. 11), and by the fact that biogenic Fe(II) is strongly sorbed. Sorption may slow the Fe(II) oxidation rate or prevent microscopic migration to oxidizing Mn oxide surfaces. Although the form of Fe(II) responsible for TcO_4^- reduction is currently unknown, it is clear that it is solid phase-associated since the concentrations of aqueous Fe(II) were at or below detection in all of the sediment suspensions regardless of the concentration of HCl extractable Fe(II).

In each of the three sediments investigated as part of this study, the rate of abiotic TcO_4^- reduction was related to the extent of Fe(III) bioreduction as determined by the concentration of 0.5 N HCl extractable Fe(II). The initial rates of abiotic TcO_4^- reduction in all the microbially reduced sediments were first-order but at the later stages of reduction the rate order changed as the reduction rate slowed. The reasons for this are currently unknown but may be related to a decreasing concentration of reactive sites where sufficient Fe(II) ions are coordinated in a manner to facilitate the $3e^-$ transfer required to reduce Tc(VII) to Tc(IV). For each sediment, the initial rate, expressed as a first-order rate constant, was related to the HCl-extractable Fe(II) concentration with the rate of TcO_4^- reduction increasing with increasing Fe(II) (Table 3 and Fig. 13). The first-order reduction rates for TcO_4^- (in h^{-1}) in both the Eatontown and Ringold sediments correlated well with 0.5 N HCl extractable Fe(II) and defined a single relationship with steep slope (Fig. 13). Reduction rates for TcO_4^- in the bioreduced FRC sediment also correlated with acid extractable Fe(II), but the relationship defined was completely different from that observed for the other two sediments. Solid phase-associated, biogenic Fe(II) was much less reactive in the FRC sediment.

The homogeneous reduction of TcO_4^- to Tc(IV) by $Fe^{2+}_{(aq)}$ is thermodynamically feasible at circumneutral pH under certain conditions. The $TcO(OH)_2$ aqueous species is the dominant one in contact with $TcO_2 \cdot nH_2O(s)$ over the pH range of 3–9 (Rard et al., 1999), where its concentration remains relatively constant at 10^{-8} mol/L (given effects of ionic strength, etc.). Given this aqueous complex, the Tc(VII)/Tc(IV) couple may be restated as follows:

$$TcO_4^- + 4H^+ + 3e^- = TcO(OH)_{2(aq)} + H_2O \qquad (2)$$

with $E^o = 0.579$ V and log K (298) = 29.4 (Rard et al., 1999). Implicit in this reaction is the solubility of $TcO_2 \cdot nH_2O(s)$. Factoring in the half-cell reaction for $Fe^{2+}/Fe(OH)_3$ [$E^o = 1.01$ V, log K (298) = 17.06] yields the following overall oxidation-reduction reaction for TcO_4^-:

$$TcO_4^- + 3Fe^{2+}_{(aq)} = TcO(OH)_{2(aq)} + Fe(OH)_3 + 5H^+ \qquad (3)$$

with log K (298) = −21.8. The stoichiometry of Eqn. 3

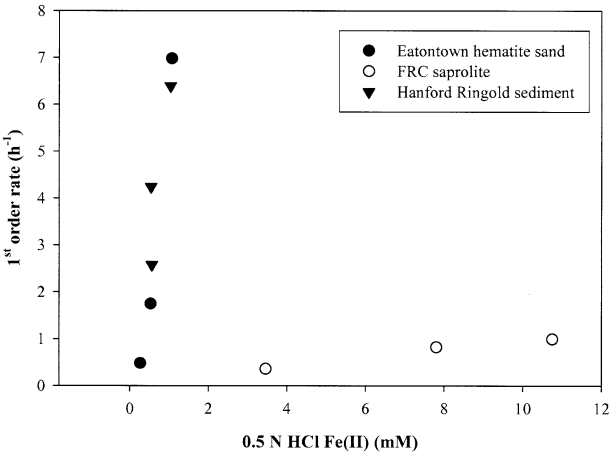

Fig. 13. The relationship of first-order rate constants for TcO_4^- reduction to total biogenic Fe(II) extracted by 0.5 N HCl. The Ringold data were taken from the 1.0 g experiments after 35 and 43 d of bioreduction. These particular experiments showed low variance between replicates, and 0.5 N HCl Fe(II) was measured on the bioreduced sediments. The data for the FRC and Eatontown sediments are from Table 3.

displays that the thermodynamic feasibility of TcO_4^- reduction by the aqueous ferrous ion is a strong function of pH and $Fe^{2+}_{(aq)}$ concentration. Equation 3 can be used with its log K to show that at pH ≈7 and with Fe^{2+} concentrations of 10^{-3} and 10^{-6} mol/L, homogeneous reduction will occur when TcO_4^- concentrations exceed $10^{-12.2}$ and $10^{-3.2}$ mol/L, respectively. The kinetic feasibility of homogeneous reduction, however, is in doubt as Cui and Eriksen (1996b) observed that TcO_4^- reduction by $Fe^{2+}_{(aq)}$ to $TcO_2 \cdot nH_2O_{(s)}$ proceeded slowly or not at all. These findings are consistent with unpublished results from our laboratory where 40 μM $Fe^{2+}_{(aq)}$ in pH 7 PIPES buffer equilibrated with 0.25 μM TcO_4^- for periods up to 10 d resulted in no significant decrease in $TcO^-_{4\,(aq)}$ concentration. A thermodynamic calculation for these specific conditions suggested that reduction should occur when TcO_4^- was greater than approximately 10^{-8} mol/L.

In contrast to $Fe^{2+}_{(aq)}$, TcO_4^- is heterogeneously reduced by a variety of Fe(II)-containing minerals including $Fe(OH)_2$, chlorite, siderite ($FeCO_3$), and magnetite (Fe_3O_4) (Cui and Eriksen, 1996b; Vandergraaf et al., 1984; Winkler et al., 1988). Lloyd et al. (2000) demonstrated that TcO_4^- was reduced by a nanocrystalline magnetite generated via biotic reduction of a poorly crystalline Fe(III) oxide by *Geobacter sulfurreducens*. Our experience with biogenic magnetites indicates that they often contain a significant sorbed Fe(II) component (Kukkadapu et al., 2003; Zachara et al., 2002).

In the experiments reported herein, there was inconclusive evidence for the formation of biogenic Fe(II) solids as a result of the bioreduction of sediment-associated Fe(III). Siderite ($FeCO_3$) formation was plausible given the use of 30 mM bicarbonate to buffer pH, and the generation of mM concentrations of Fe(II) by bacterial reduction. We have observed siderite precipitation in previous anoxic incubations of discrete Fe(III) oxides with CN32 in bicarbonate buffer (Fredrickson et al., 1998; Zachara et al., 1998; Zachara et al., 2001). A common attribute of the sediment bioreduction experiments reported herein was the virtual absence of Fe(II) release to the aqueous phase, indicating precipitation or strong adsorption. We have used the general term "sorption" to describe the retention of Fe(II) by the solid phase because the measurements reported herein did not allow definitive identification of chemical form. The lack of Fe(II) Mössbauer signal in the bioreduced Eatontown sediment, where the lowest levels of Fe(II) were generated, suggested that solid phase–associated Fe(II) existed in an adsorbed state, most probably to residual hematite. Fe(II) is sorbed strongly by crystalline Fe(III) oxides at circumneutral pH (Jeon et al., 2001; Zachara et al., 2000), and can exhibit irreversible adsorption behavior (Jeon et al., 2001). In contrast, the peak positions of Fe(II) in the 77°K Mössbauer spectrum of the bioreduced Ringold sediment (Fig. 5c) provided presumptive evidence for the formation of siderite. This interpretation was supported by the co-observance of rhodochrosite ($MnCO_3$) in this same sample (data not shown). The presence of significant residual goethite in the bioreduced Ringold sediment (Fig. 5c) indicated that adsorbed Fe(II) probably existed in this material as well. With bioreduction, the FRC sediment showed significant increase in its 77°K Mössbauer peak attributed to Fe(II) (Fig. 3a,c). The biogenic Fe(II) exhibited a peak position common to that attributed to phyllosilicate Fe(II) in the pristine sediment (Fig. 3b). However, a variety of Fe(II) compounds including siderite, green rusts, and others yield peaks in this position (see for example, Kukkadapu et al., 2003), preventing unambiguous identification. Lastly, the extent of Fe(II) associated with the surface of *S. putrefaciens* CN32 cells added to the sediments in these studies is unknown but could potentially have a role in the observed redox reactions. Given the relatively high surface area of bacterial cells and their capacity for binding cationic metals, the reactivity of cell surface–associated Fe(II) warrants further investigation.

Our results indicated that solid phase–associated Fe(II) [precipitated and Fe(III) oxide- or cell-adsorbed] reduced $Tc(VII)O_4^-$ relatively rapidly to insoluble $Tc(IV)O_2 \cdot nH_2O$. Others have reported that sorbed Fe(II) is also an effective contaminant reductant (Amonette et al., 2000; Haderlein and Pecher, 1999; Klausen et al., 1995). Fe(II) sorbed onto goethite (α-FeOOH) (Fredrickson et al., 2000) or hematite (α-Fe_2O_3) (Liger et al., 1999) has been shown to reduce U(VI), while Fe(II) sorbed on the surface of an untreated glass reaction vessel or on quartz reacted with TcO_4^- (Cui and Eriksen, 1996b). Fracture fill material from Stripa Mine, Sweden containing granite, hornblende, and magnetite reduced TcO_4^- from solution at a rate proportional to the surface area and Fe(II) content of the solid (Cui and Eriksen, 1996a). Because the reduction of TcO_4^- to $TcO_2 \cdot nH_2O$ requires three electrons, the density of Fe^{2+} as either a sorbed species or mineral precipitate is likely to be an important, if not critical factor controlling the kinetics of the reduction reaction (Cui and Eriksen, 1996b).

A curious finding was the uniform dependence of the first-order reduction rate on total biogenic Fe(II) in the Ringold and Eatontown sediments and a disparate correlation for the FRC sediment (Fig. 13). We hypothesize that this is due to a different mineralogic association of biogenic Fe(II) in the Ringold and Eatontown sediments as compared to the FRC. Our understanding of the complex mineralogy and surface chemistry of these sediments is currently insufficient to address this hypothesis, but speculation can be made. The Eatontown and Ringold sediments exhibit a common geologic character, they are both comprised of sand and silt sized quartz grains and aluminosilicate lithic fragments with extensive crystalline Fe(III) oxide precipitates on grain surfaces. The primary Fe(II) sorbents in these materials were the crystalline Fe(III) oxides goethite and hematite. It is probable that the heterogeneous reduction reaction of TcO_4^- occurred through reaction with adsorbed Fe(II) on these surfaces as implied by the XMP map of the Ringold sediment in Figure 12 and similarly for the Eatontown sediment (not shown). The FRC sediment, in contrast, was comprised of variably cemented sand and silt-sized aggregates of silt and clay sized materials (Fig. 11, BSE image). Unlike the other two sediments, phyllosilicates (illite, vermiculite, and smectite) were major mineralogic components of FRC material. The distribution of Tc(IV) (Fig. 11) showed significant intra-aggregate penetration of Tc and qualitatively greater association with Fe-poor regions. It is possible that the slower reduction rates noted for FRC material resulted from intra-aggregate diffusion to reactive Fe(II) containing areas, and from the adsorption of Fe(II) by mineral phases other than goethite in the sediment. Biogenic Fe(II) was noted to be desorbable, in part, by an aqueous $CaCl_2$ electrolyte implying potential association with the phyllosilicate fraction. The forms of sediment-associated

Fe(II) responsible for heterogeneous pertechnetate reduction are now being investigated in greater detail in our laboratory.

5. ENVIRONMENTAL IMPLICATIONS

Fe(II) generated as a result of microbial reduction of sediment-associated Fe(III) was found to be a facile reductant of $TcO_{4\,(aq)}^-$ with the initial rate of Tc(VII) reduction increasing with increasing concentrations of HCl-extractable Fe(II) in each of the subsurface materials examined. Although the reactive form(s) of Fe(II) were not identified, the fact that this reaction was observed in three distinct subsurface materials suggests that results can be generalized to a broad range of subsurface environments. Two of the three materials were from the Department of Energy's Hanford and Oak Ridge Sites where Tc migration is a major environmental concern, and our results have specific implications to $^{99}TcO_4^-$ migration in groundwater at these locations. Although the formation of soluble Tc(IV) carbonate complexes during microbial enzymatic reduction has previously been reported (Wildung et al., 2000), there was no evidence of the formation of such a complex during reduction by biogenic Fe(II) in the current studies despite the use of 30 mM $NaHCO_3$ as a pH buffer. It should also be pointed out that all of the experiments reported herein were conducted at 25°C. Although this temperature is 5–10°C warmer than most aquifer temperatures in the continental U.S., it is expected that this temperature difference would have only a minor effect on the abiotic redox reactions observed herein.

Although the direct enzymatic reduction of Tc has been demonstrated for a range of organisms (Lloyd et al., 1997; Lloyd and Macaskie, 1996; Lloyd et al., 1999; Wildung et al., 2000), the development of an effective in situ remediation approach based on this biologic process could prove challenging. At Hanford, the unconfined aquifer is oligotrophic and supports a relatively low biomass–low activity microbial community (Kieft et al., 1995). Increasing the in situ microbial biomass or activity levels and sustaining them over extended periods that would be required for continuous reduction of contaminants is likely to be technically challenging and costly. An alternative approach that may prove more practical and effective would be to reduce sediment-associated Fe(III), thereby creating a permeable barrier of reactive Fe(II) that would remove TcO_4^- via heterogeneous reduction as contaminated groundwater migrates through the reduced zone. Our findings suggest that very little of the Fe(II) produced via microbial reduction of sediment Fe(III) in these particular sediments is solubilized (e.g., Fig. 2). The Fe(III) remains associated with the solid phase, and is most likely adsorbed to, or precipitated on, particle surfaces. Hence, a significant fraction of the Fe(II) produced remains in place as a kinetically reactive phase.

A permeable in situ redox barrier, generated via abiotic reduction of Fe(III) with dithionite, was successfully demonstrated at the Hanford Site for the removal of Cr(VI) from solution by reduction to relatively insoluble Cr(III) (Fruchter et al., 2000). In situ microbial reduction of Fe(III) should also be feasible, requiring relatively benign organic compounds to stimulate microbial activity. Caccavo et al. (1996) demonstrated the feasibility of this process by stimulating the reduction of Fe(III) in Hanford subsurface sediments by resuscitating starved *Shewanella alga* BrY cells and then observing the rapid abiotic reduction of Cr(VI).

The results presented herein are also applicable to subsurface environments that are naturally reduced. At Hanford, the upper portions of the unconfined aquifer are predominantly aerobic, but it is unclear whether aerobic conditions extend continuously to the base of the aquifer. Geomicrobial studies of core samples collected at depth indicate that there are low permeability zones containing populations of viable dissimilatory Fe(III)- and sulfate-reducing bacteria and significant concentrations, as high as 4 g kg^{-1}, of 0.5 N HCl-extractable Fe(II) (McKinley et al., 1997).

Although the in situ reduction of Fe(III) to create permeable barriers to contaminant migration holds considerable promise for treatment of Cr-contaminated groundwater (Fruchter, 2002), the susceptibility of $TcO_2 \cdot nH_2O$ to oxidation calls into question the long-term stability of this phase in the absence of continuous maintenance of reducing conditions. In contrast to $Cr(OH)_3$ that does not readily react with O_2, $TcO_2 \cdot nH_2O$ oxidizes to soluble Tc species in air-equilibrated circumneutral solutions (unpublished results). The behavior of $TcO_2 \cdot nH_2O_{(s)}$ with respect to O_2 oxidation in sediments is, however, uncertain. This is illustrated by the results of experiments investigating the oxidation of Tc from Fe(II)-facilitated TcO_4^- reduction where Cui and Eriksen (1996a) observed only minor increases in soluble Tc corresponding to the solubility of $TcO_2 \cdot nH_2O$ over a period of 3 weeks in air-saturated groundwater. The explanation offered for this observation was that oxidation of the reduced Tc was suppressed by competing reactions between O_2 and residual Fe(II). It will be important therefore to define not only the reactive forms of biogenic Fe(II) in subsurface materials but also the capacity of these materials for contaminant reduction and potential for buffering against oxidation. This information will be critical for predicting the effectiveness and longevity of contaminant redox barriers in the subsurface.

Acknowledgments—This research was supported by the Natural and Accelerated Bioremediation Research Program (NABIR), Office of Biologic and Environmental Research (OBER), U.S. Department of Energy (DOE). Pacific Northwest National Laboratory (PNNL) is operated for the DOE by Battelle Memorial Institute under Contract DE-AC06-76RLO 1830. We wish to acknowledge the insightful comments of three anonymous reviewers and to thank Alice Dohnalkova (PNNL) for excellent assistance on the high-resolution transmission electron microscopy analyses, Hailiang Dong (Miami University–Ohio) for SEM images, and David Boone (Portland State University) for providing *S. putrefaciens* CN32 to us from the Subsurface Microbial Culture Collection. The PNC-CAT facilities are supported by the U.S. Department of Energy, Office of Science Grant DE-FG03-97ER45628. Use of the Advanced Photon Source was supported by the U.S. Department of Energy, Office of Science, Office of Basic Energy Sciences, under Contract W-31-109-ENG-38. Appreciation is extended to Dr. Nancy Hess of PNNL who provided XANES reference spectra for $TcO_{4\,(aq)}^-$ and $TcO_2 \cdot nH_2O_{(s)}$. Mössbauer analyses were performed within the W. R. Wiley Environmental Molecular Sciences Laboratory (EMSL), a national scientific user facility sponsored by the U.S. Department of Energy's Office of Biological and Environmental Research and located at PNNL. PNNL is operated for the Department of Energy by Battelle.

Associate editor: J. B. Fein

REFERENCES

Amonette J. E., Workman D. J., Kennedy D. W., Fruchter J. S., and Gorby Y. A. (2000) Dechlorination of carbon tetrachloride by Fe(II) associated with goethite. *Environ. Sci. Technol.* **34** (*21*)**,** 4606–4613.

Bancroft G. M. (1973) Mössbauer Spectroscopy: An Introduction for Inorganic Chemists and Geochemists. McGraw-Hill.

Burdige D. J. and Nealson K. H. (1986) Chemical and microbiological studies of sulfide-mediated manganese reduction. *Geomicrobiol. J.* **4** (*4*)**,** 361–387.

Caccavo F., Ramsing N. B., and Costerton J. W. (1996) Morphological and metabolic responses to starvation by the dissimilatory metal-reducing bacterium *Shewanella alga* BrY. *Appl. Environ. Microbiol.* **62** (*12*)**,** 4678–4682.

Cui D. and Eriksen T. E. (1996a) Reduction of pertechnetate in solution by heterogeneous electron transfer from Fe(II)-containing geological material. *Environ. Sci. Technol.* **30,** 2263–2269.

Cui D. and Eriksen T. E. (1996b) Reduction of pertechnetate by ferrous iron in solution: Influence of sorbed and precipitated Fe(II). *Environ. Sci. Technol.* **30,** 2259–2262.

Fendorf S. E. and Zasoski R. J. (1992) Chromium(III) oxidation by δ-MnO_2. *Environ. Sci. Technol.* **26,** 79–85.

Fredrickson J. K., Zachara J. M., Kennedy D. W., Dong H., Onstott T. C., Hinman N. W., and Li S. W. (1998) Biogenic iron mineralization accompanying the dissimilatory reduction of hydrous ferric oxide by a groundwater bacterium. *Geochim. Cosmochim. Acta* **62** (*19/20*)**,** 3239–3257.

Fredrickson J. K., Zachara J. M., Kennedy D. W., Duff M. C., Gorby Y. A., Li S. W., and Krupka K. M. (2000) Reduction of U(VI) in goethite (α-FeOOH) suspensions by a dissimilatory metal-reducing bacterium. *Geochim. Cosmochim. Acta* **64,** 3085–3098.

Fredrickson J. K., Zachara J. M., Kennedy D. W., Liu C., Duff M. C., Hunter D. B., and Dohnalkova A. (2002) Influence of Mn oxides on the reduction of Uranium(VI) by the metal-reducing bacterium *Shewanella putrefaciens*. *Geochim. Cosmochim. Acta* **66** (*18*)**,** 3247–3262.

Fredrickson J. K., Zachara J. M., Kukkadapu R. K., Gorby Y. A., Smith S. C., and Brown C. F. (2001) Biotransformation of Ni-substituted hydrous ferric oxide by an Fe(III)-reducing bacterium. *Environ. Sci. Technol.* **35,** 703–712.

Fruchter J. (2002) In situ treatment of chromium-contaminated groundwater. *Environ. Sci. Technol.* **36,** 464A–472A.

Fruchter J. S., Cole C. R., Williams M. D., Vermeul V. R., Amonette J. E., Szecsody J. E., Istok J. D., and Humphrey M. D. (2000) Creation of a subsurface permeable treatment zone for aqueous chromate contamination using in situ redox manipulation. *Ground Water Monitoring and Remediation* **20** (*2*)**,** 66–77.

Gorby Y. A., Caccavo J. F., and Bolton H., Jr.. (1998) Microbial reduction of $cobalt^{III}EDTA^{-}$ in the presence and absence of manganese(IV) oxide. *Environ. Sci. Technol.* **32,** 244–250.

Haderlein S. B. and Pecher K. (1999) Pollutant reduction in heterogeneous Fe(II)-Fe(III) systems. In *Mineral–Water Interfacial Reactions: Kinetics and Mechanisms* (ed. D. L. Sparks and T. J. Grundl), pp. 342–356. American Chemical Society.

Heron G. and Christensen T. H. (1995) Impact of sediment-bound iron on redox buffering in a landfill leachate polluted aquifer (Vejen, Denmark). *Environ. Sci. Technol.* **29,** 187–192.

Jeon B. H., Dempsey B. A., Burgos W. D., and Royer R. A. (2001) Reactions of ferrous iron with hematite. *Colloids and Surfaces A: Physicochemical and Engineering Aspects* **191,** 41–55.

Kieft T. L., Fredrickson J. K., McKinley J. P., Bjornstad B. N., Rawson S. A., Phelps T. J., Brockman F. J., and Pfiffner S. M. (1995) Microbiological comparisons within and across contiguous lacustrine, paleosol, and fluvial subsurface sediments. *Appl. Environ. Microbiol.* **61** (*2*)**,** 749–757.

Klausen J., Trober S. P., Haderlein S. B., and Schwarzenbach R. P. (1995) Reduction of substituted nitrobenzenes by Fe(II) in aqueous mineral suspensions. *Environ. Sci. Technol.* **29 (***9***),** 2396–2404.

Kukkadapu R. K., Zachara J. M., Fredrickson J. K., Smith S. C., Dohnalkova A., and Russell C. K. (2003) Transformation of 2-line ferrihydrite to 6-line ferrihydrite under oxic and anoxic conditions . *Am. Mineralogist* **88,** 1903–1914.

Kukkadapu R. K., Zachara J. M., Smith S. C., Fredrickson J. K., and Liu C. (2001) Dissimilatory bacterial reduction of Al-substituted goethite in subsurface sediments. *Geochim. Cosmochim. Acta* **65,** 2913–2924.

Lee S. Y., Phillips D. H., Ammons J. T., and Lietzke D. A. (1990) A microscopic study of iron and manganese oxide distribution in soils from East Tennessee (U.S.A.). In *Soil Micromorphology: A Basic and Applied Science* (ed. L. A. Douglas), pp. 511–517. Elsevier Science.

Liger E., Charlet L., and Van Cappellen P. (1999) Surface catalysis of uranium(VI) reduction by Fe(II). *Geochim. Cosmochim. Acta* **63,** 2939–2955.

Liu C., Zachara J. M., Fredrickson J. K., Kennedy D. W., and Dohnalkova A. (2002) Modeling the inhibition of the bacterial reduction of U(VI) by β-$MnO_{2(s)}$. *Environ. Sci. Technol.* **36,** 1452–1459.

Lloyd J. R., Cole J. A., and Macaskie L. E. (1997) Reduction and removal of heptavalent technetium from solution by *Escherichia coli*. *J. Bacteriol.* **179,** 2014–2021.

Lloyd J. R. and Macaskie L. E. (1996) A novel phosphorimager-based technique for monitoring the microbial reduction of technetium. *Appl. Environ. Microbiol.* **62** (*2*)**,** 578–582.

Lloyd J. R., Ridley J., Khizniak T., Lyalikova N. N., and Macaskie L. E. (1999) Reduction of technetium by *Desulfovibrio desulfuricans*: Biocatalyst characterization and use in a flowthrough bioreactor. *Appl. Environ. Microbiol.* **65,** 2691–2696.

Lloyd J. R., Sole V. A., Van Praagh C. V. G., and Lovley D. R. (2000) Direct and Fe(II)-mediated reduction of technetium by Fe(III)-reducing bacteria. *Appl. Environ. Microbiol.* **66** (*9*)**,** 3743–3749.

Lovley D. R. and Phillips E. J. P. (1988) Manganese inhibition of microbial iron reduction in anaerobic sediments. *Geomicrobiol. J.* **5,** 145–155.

McKinley J. P., Stevens T. O., Fredrickson J. K., Zachara J. M., Colwell F. S., Wagnon K. B., Rawson S. A., and Bjornstad B. N. (1997) The biogeochemistry of anaerobic lacustrine and paleosol sediments within an aerobic unconfined aquifer. *Geomicrobiol. J.* **14,** 23–39.

Myers C. R. and Nealson K. H. (1988) Microbial reduction of manganese oxides: Interactions with iron and sulfur. *Geochim. Cosmochim. Acta* **52,** 2727–2732.

Ono K. and Ito A. (1964) Mössbauer study of magnetic properties in ferrous compounds. *J. Phys. Chem.* **19,** 899–907.

Phillips D. H., Ammons J. T., Lee S. Y., and Lietzke D. A. (1998) Deep weathering of calcareous sedimentary rock and the redistribution of iron and manganese in soil and saprolite. *Soil Sci.* **163** (*1*)**,** 71–81.

Phillips D. H., Ammons J. T., Lietzke D. A. and Lee S. Y. (1997) Morphology and mineralogy of saprolite and selected soils from the Maryville limestone and Nolichucky shale formations in East Tennessee. *Soil Survey Horizons* 107–120.

Rard J. A., Rand M. H., Anderegg G., and Wanner H. (1999) Chemical Thermodynamics of Technetium. Elsevier Science.

Riley R. G. and Zachara J. M. (1992) Chemical contaminants on DOE lands and selection of contaminant mixtures for subsurface science research. U.S. Department of Energy, Washington, D.C.

Serne R. J., Last G. V., Gee G. W., Schaef H. T., Lanigan D. C., Lindenmeier C. W., Clayton R. E., LeGore V. L., Orr R. D., O'Hara M. J., Brown C. F., Burke D. B., Owen A. T., Kutnyakov I. V. and Wilson T. C. (2001a). Geologic and geochemical data collected from vadose zone sediments from borehole SX 41-09-39 in the S/SX waste management area and preliminary interpretations. *PNNL-2001–2.* Pacific Northwest National Laboratory.

Serne R. J., Schaef H. T., Bjornstad B. N., Lanigan D. C., Gee G. W., Lindenmeier C. W., Clayton R. E., LeGore V. L., O'Hara M. J., Brown C. F., Orr R. D., Last G. V., Kutnyakov I. V., Burke D. B., Wilson T. C. and Williams B. A. (2001b). Geologic and geochemical data collected from vadose zone sediments from borehole 299 W23-19 [sx-115] in the S/SX waste management area and preliminary interpretations. *PNNL-2001–3.* Pacific Northwest National Laboratory.

Serne R. J., Schaef H. T., Last G. V., Lanigan D. C., Lindenmeier C. W., Clayton R. E., LeGore V. L., O'Hara M. J., Brown C. F., Orr R. D., Kutnyakov I. V., Wilson T. C., Burke D. B., Williams B. A. and Bjornstad B. N. (2001c). Geologic and geochemical data collected from vadose zone sediments from the slant borehole under

SX-108 in the S/SX waste management area and preliminary interpretations. *PNNL-2001–4*. Pacific Northwest National Laboratory.

Stone A. T. (1987) Microbial metabolites and the reductive dissolution of manganese oxides—oxalate and pyruvate. *Geochim. Cosmochim. Acta* **51** (*4*)**,** 919–925.

Stone A. T. and Morgan J. J. (1984) Reduction and dissolution of manganese(iii) and manganese(iv) oxides by organics. 2. Survey of the reactivity of organics. *Environ. Sci. Technol.* **18** (*8*)**,** 617–624.

Vandergraaf T. T., Ticknor K. V., and George I. M. (1984) Reactions between technetium in solution and iron-containing minerals under oxic and anoxic conditions. In *Geological Behavior of Radioactive Waste, Series 246* (ed. G. S. Barney), pp. 25–43. American Chemical Society, Washington, DC.

Wielinga B., Bostick B., Hansel C. M., Rosenzweig R. F., and Fendorf S. (2000) Inhibition of bacterially promoted uranium reduction: Ferric (hydr)oxides as competitive electron acceptors. *Environ. Sci. Technol.* **34** (*11*)**,** 2190–2195.

Wildung R. E., Gorby Y. A., Krupka K. M., Hess N. J., Li S. W., Plymale A. E., McKinley J. P., and Fredrickson J. K. (2000) Effect of electron donor and solution chemistry on products of dissimilatory reduction of technetium by *Shewanella putrefaciens*. *Appl. Environ. Microbiol.* **66** (*6*)**,** 2451–2460.

Winkler A., Bruhl H., Trapp C., and Bock W.-D. (1988) Mobility of technetium in various rocks and defined combinations of natural materials. *Radiochim. Acta* **44**/**45,** 183–186.

Zachara J. M., Fredrickson J. K., Li S. W., Kennedy D. W., Smith S. C., and Gassman P. L. (1998) Bacterial reduction of crystalline Fe^{3+} oxides in single-phase suspensions and subsurface materials. *Am. Miner.* **83,** 1426–1443.

Zachara J. M., Fredrickson J. K., Smith S. C., and Gassman P. L. (2001) Solubilization of Fe(III) oxide-bound trace metals by a dissimilatory Fe(III) reducing bacterium. *Geochim. Cosmochim. Acta* **65** (*1*)**,** 75–93.

Zachara J. M., Gassman P. L., Smith S. C., and Taylor D. (1995) Oxidation and adsorption of Co(II) $EDTA^{2-}$ complexes in a subsurface materials with iron and manganese oxides. *Geochim. Cosmochim. Acta* **59,** 4449–4463.

Zachara J. M., Kukkadapu R. K., Fredrickson J. K., Gorby Y. A., and Smith S. C. (2002) Biomineralization of poorly crystalline Fe(III) oxides by dissimilatory metal reducing bacteria (DMRB). *Geomicrobiol. J.* **19** (*2*)**,** 179–207.

Zachara J. M., Kukkadapu R. K., Gassman P. L., Dohnalkova A., Fredrickson J. K., Young J. S., and Anderson T. (2004) Biogeochemical transformation of Fe-minerals in a petroleum contaminated aquifer . *Geochim. Cosmochim. Acta* **68** (*8*)**,** 1791–1805.

Zachara J. M., Kukkadapu R. K., Gassman P. L., Dohnalkova A., Fredrickson J. K., Young J. S. and Anderson T. (2004). Biogeochemical transformation of Fe-minerals in a petroleum contaminated aquifer. *Geochim. Cosmochim. Acta* (Submitted).

Zachara J. M., Smith S. C., and Fredrickson J. K. (2000) The effect of biogenic Fe(II) on the stability and sorption of Co(II)$EDTA^{2-}$ to goethite and a subsurface sediment. *Geochim. Cosmochim. Acta* **64** (*8*)**,** 1345–1362.